Molecules and Clusters on Oxide Surfaces

Ataman, Evren

2011

Molecules and Clusters on Oxide Surfaces

LUND UNIVERSITY
Faculty of Science

Thesis for the Degree of Doctor of Philosophy

Evren Ataman
Division of Synchrotron Radiation Research
Department of Physics

June 2011

Doctoral Thesis
Division of Synchrotron Radiation Research
Department of Physics
Lund University

ISBN 978-91-7473-139-2
Printed by Media-Tryck
Lund, Sweden, May 2011

If you have an apple and I have an apple and we exchange these apples, then you and I still each have one apple. But if you have an idea and I have an idea and we exchange these ideas, then each of us will have two ideas.

George Bernard Shaw
Irish playwright

Preface

The booklet which you hold in your hands or display on a computer screen is the thesis which presents the results of almost five years of work performed by me and my colleagues, who are mostly located at the Division of Synchrotron Radiation Research at the Department of Physics at Lund University. The thesis consists of two parts. The first is the *Summary* part which consists of seven chapters. In the *Summary* I briefly summarize the targets, methods, materials and results of the work. The second part, the *Papers*, is a collection of seven papers which are either published, submitted to a journal, or manuscripts which are almost in their final form for submission and all together lay the foundations for this thesis.

The title of the thesis, *Molecules and Clusters on Oxide Surfaces*, is intended to underline the general topic of the work. The terms "molecules", "clusters", and "oxide surfaces" stand specifically for organic molecules – mainly amino acids –, gold clusters with a size on the nanometer scale, and the (110) and (111) surfaces of the rutile TiO_2 single crystal and of an ultrathin FeO film grown on the Pt(111) surface, respectively. The main purpose of the thesis is to contribute to the understanding of the fundamental interactions between these different substances with the methods of what is called the *surface science approach*.

In the first chapter of the *Summary* an overview of surface science and synchrotron radiation research is given. The motivation for this work is presented, by explaining organic-inorganic interfaces, catalysis, and dye-sensitized solar cells. In the second chapter X-ray photoelectron spectroscopy (XPS), X-ray absorption spectroscopy (XAS), scanning tunneling microscopy (STM), and density functional theory (DFT) are described briefly. In the third chapter important properties of the *L*-cysteine, *L*-cystine, S-methyl-*L*-cysteine, and the Zinc-protoporphyrin IX molecules are presented, and likewise those of the rutile TiO_2(110) and FeO(111)/Pt(111) surfaces and gold clusters. Relevant literature is cited. In the fourth chapter the results of the thesis are summarized and most interesting points are highlighted. In the fifth chapter the results are put into a wider perspective, and possible future work is commented on. The *Summary* part is concluded by references and acknowledgments.

In the *Summary* I tried to comment about all relevant issues related to my work. However, I have omitted certain topics intentionally. I have used low energy electron diffraction (LEED) only in a qualitative manner to validate certain structures, but I have never employed it as a major technique to acquire further information and therefore no description is of this technique is included in the *Summary*. Electrospray deposition is a very convenient technique to deposit large molecules onto surfaces in ultrahigh vacuum, which cannot be sublimated by standard thermal methods. This method is used in **Paper 6.** Since I have not used it extensively I did not included any description of this technique, either. Further, I do not discuss any details about the electronics of the instruments I have been using. I have performed DFT calculations using the CASTEP code. I have a working knowledge of the code and parallel computing methods, but I have not dealt with the code on a too detailed level and therefore do not discuss these details.

The *Papers* part consists of seven papers. In **Paper 1** the results of an XPS study are presented, in which the adsorption of submono- to multilayers of *L*-cysteine on the rutile TiO_2(110) surface is investigated. **Paper 2** extends the study of **Paper 1** to the co-adsorption of gold and *L*-cysteine on the

rutile TiO_2(110) surface. The method used is, again, XPS. In **Paper 3** DFT is employed to gain more detailed information on the adsorption structure of *L*-cysteine molecules on the TiO_2(110) surface. In **Paper 4** the adsorption of two different amino acids, *L*-cystine and S-methyl-*L*-cysteine, on the TiO_2(110) surface, is investigated by XPS. In **Paper 5** XPS results of an "unconventional" zwitterionic state of *L*-cysteine multilayers are reported. In **Paper 6** the adsorption of a dye Zinc-protoporphyrin IX on the TiO_2(110) surface is studied by XPS and XAS. In **Paper 7** STM and XPS are used to study the adsorption of gold clusters on a partly reduced ultrathin FeO(111). The paper also contains results on the adsorption of CO on this surface.

List of Papers

Results of the work which has been performed during my PhD education are presented in the following papers, which lay the foundation of this thesis. I was main responsible for carrying out the experiments, analyzing the data, and writing the manuscripts of **Paper 1**, **Paper 2**, and **Paper 4**. I carried out the DFT calculations and wrote the manuscript of **Paper 3**. I was main responsible for conducting the experiments and analyzing the data and have participated in the writing of **Paper 5**. I took part in the experimental work of **Papers 6** and **Paper 7**.

Paper 1
E. Ataman, C. Isvoranu, J. Knudsen, K. Schulte, J. N. Andersen, and J. Schnadt, *Adsorption of L-cysteine on rutile TiO_2(110)*, Surf. Sci. **605**, 179 (2011).

Paper 2
E. Ataman, C. Isvoranu, J. Knudsen, K. Schulte, J. N. Andersen, and J. Schnadt, *Co-adsorption of L-cysteine and gold clusters on the rutile TiO_2(110) surface*, submitted to Langmuir.

Paper 3
E. Ataman, J. Carrasco, J. N. Andersen, A. Michaelides, and J. Schnadt, *Assessment of the adsorption geometry of L-cysteine on the stoichiometric and reduced rutile TiO_2(110) surfaces by density functional theory*, in manuscript.

Paper 4
E. Ataman, C. Isvoranu, J. Knudsen, J. N. Andersen, and J. Schnadt, *Adsorption of L-cystine and S-methyl-L-cysteine on the rutile TiO_2(110) surface*, in manuscript.

Paper 5
E. Ataman, C. Isvoranu, J. N. Andersen, J. Schnadt, and K. Schulte, *Unconventional zwitterionic state of cysteine*, submitted to J. Am. Chem. Soc.

Paper 6
A. Rienzo, L. C. Mayor, G. Magnano, C. J. Satterley, **E. Ataman**, J. Schnadt, K. Schulte, and J. N. O'Shea, *X-ray absorption and photoemission spectroscopy of Zinc-protoporphyrin adsorbed on rutile TiO_2(110) prepared by in situ electrospray deposition*, J. Chem. Phys. **132**, 084703 (2010).

Paper 7
J. Knudsen, K. Schulte, **E. Ataman**, C. Isvoranu, J. N. Andersen, and J. Schnadt, *Tuning the CO adsorption properties on Au-particles supported by a partly reduced FeO(111) film*, in manuscript.

In addition to my own project, I have had the chance of being involved in several different projects, to which I have contributed at different levels. My contribution to the following work, which is not included in the thesis, is mirrored by the position of my name in the author list.

Paper 8
S. Weigelt, J. Schnadt, A. K. Tuxen, F. Masini, C. Bombis, C. Busse, C. Isvoranu, **E. Ataman**, E. Lægsgaard, F. Besenbacher, and T. R. Linderoth, *Formation of trioctylamine from octylamine on Au(111)*, J. Am. Chem. Soc. **130**, 5388 (2008)

Paper 9
C. Isvoranu, J. Åhlund, B. Wang, **E. Ataman**, N. Mårtensson, C. Puglia, J. N. Andersen, M.-L. Bocquet, and J. Schnadt, *Electron spectroscopy study of the initial stages of iron phthalocyanine growth on highly oriented pyrolitic graphite,* J. Chem. Phys. **131**, 214709 (2009)

Paper 10
A. Shavorskiy, T. Eralp, **E. Ataman**, C. Isvoranu, J. Schnadt, J. N. Andersen, and G. Held, *Dissociation of water on oxygen-covered Rh{111}*, J. Chem. Phys. **131**, 214707 (2009)

Paper 11
C. Isvoranu, B. Wang, K. Schulte, **E. Ataman**, J. Knudsen, J. N. Andersen, M.-L. Bocquet, and J. Schnadt, *Tuning the spin state of iron phthalocyanine by ligand adsorption*, J. Phys.: Condens. Matter **22**, 472002 (2010)

Paper 12
C. Isvoranu, B. Wang, **E. Ataman**, K. Schulte, J. Knudsen, J. N. Andersen, M.-L. Bocquet, and J. Schnadt, *Ammonia adsorption on iron phthalocyanine on Au(111): Influence on adsorbate-substrate coupling and molecular spin*, J. Chem. Phys. **134**, 114710 (2011)

Paper 13
C. Isvoranu, J. Knudsen, **E. Ataman**, K. Schulte, B. Wang, M.-L. Bocquet, J. N. Andersen, and J. Schnadt, *Adsorption of Ammonia on Multilayer Iron Phthalocyanine*, J. Chem. Phys. **134**, 114711 (2011)

Paper 14
C. Isvoranu, B. Wang, **E. Ataman**, J. Knudsen, K. Schulte, J. N. Andersen, M.-L. Bocquet, and J. Schnadt, *Comparison of the Carbonyl and Nitrosyl Complexes Formed by Adsorption of CO and NO on Monolayers of Iron Phthalocyanine on Au(111)*, submitted to J. Phys. Chem. C.

Paper 15
C. Isvoranu, B. Wang, **E. Ataman**, K. Schulte, J. Knudsen, J. N. Andersen, M.-L. Bocquet, and J. Schnadt, *Pyridine Adsorption on Single-Layer Iron Phthalocyanine on Au(111)*, submitted to J. Phys. Chem. C.

Contents

Part 1
Summary

Chapter 1

Introduction

This chapter serves two purposes. The first purpose is to briefly describe the importance of surfaces for the physical and chemical properties of materials, the connection between the idealized systems of surface science studies and the "real world", the applicability of results of surface science studies to real life phenomena, and the effect of synchrotron radiation facilities on surface science. The second purpose is to show why my colleagues and I thought that the systems which are investigated in this thesis were worthy concentrating and doing research on, in other words, to show what the motivation is for the work of the present thesis.

1.1 Surface Science and Synchrotron Radiation Research

Any real solid material, whether it is studied in a laboratory or used in industry for a specific purpose or as a component in a device, is confined by surfaces. It is therefore clear that any interaction of a solid material with its environment takes place primarily at the material's surface. This implies that many properties of the materials are influenced by their surfaces. The chemical reactions which occur or are initiated at the surfaces and the effects of the surface atomic and electronic structure on the energetics and kinetics of these chemical reactions are numerous and important. For example, the differing corrosive behavior of metals is, to a large extent, determined by the metals' surface properties. Hence, surface science aimed at studying corrosion is directly relevant to one of the most important issues in industrial and technological applications of metals. Interactions of organic molecules with inorganic substances (see subsection 1.2.1), heterogeneous catalysis (see subsection 1.2.2), photochemical reactions and charge dynamics (see subsection 1.2.3), oxidation, and many more chemical processes are all intimately related to surface structure. Moreover, mechanical properties such as friction, adhesion, hardness, wettability etc., which are usually considered to be macroscopic phenomena, have their origin on the atomic scale and are strongly surface structure-dependent. Often, a surface of a material has electronic and geometrical properties which differ from those of the material's bulk. Therefore surface studies are crucial for a thorough understanding of a material's properties and function. The immense importance of surfaces to chemical reactions and physical processes has turned surface science into a common playground of physicists and chemists, which in its modern form has existed for more than four decades[1].

Many commonly used experimental surface science techniques employ electrons as a probe in the determination of surface properties. Using electrons has both advantages and disadvantages. On the one hand, electrons are easily produced, and at electron energies typically used in surface science studies they have a very low inelastic mean free path (IMFP) which is a measure of the distance a

[1] The modern era of surface science started during the 1960s and 1970s [1].

particle on average can travel in a medium without loosing its energy. For example, electrons with kinetic energies of ~50-100 eV have IMFP values of ~5-10 Å. Low IMFP assures that the probe electrons with certain energies can penetrate only a few atomic layers of the materials without loosing their energy and, likewise, that only non-scattered or elastically scattered electrons can emerge from the surface region. Electrons can easily be accelerated and focused with electric or magnetic fields and, with the correct choice of energy they can be diffracted from ordered structures on the atomic scale. On the other hand, since electrons are easily absorbed and scattered not only by the investigated material, but also any surrounding medium, high vacuum conditions (pressures ~10^{-4} mbar) are required whenever low energy electrons are employed.

A truly reliable determination of the chemical, geometrical, and electronic structure of a surface is possible only for very well-defined surfaces. Therefore surfaces used in surface science studies are very often produced by growing – or cutting – single crystals materials in certain directions. In ambient conditions any surface, apart from the most inert ones, will essentially immediately be covered by residual gas adsorbates. This issue is circumvented by performing all experiments in ultrahigh vacuum (UHV) conditions, which are good enough to keep a surface clean for a sufficiently long time, a couple of minutes for the most active surfaces and a couple of days for the most inert ones. Different samples, once introduced into an UHV chamber, can be cleaned from unwanted contaminations by application of well-established cleaning procedures. However, what is created in a UHV chamber is very different from what exists under real conditions. For example, in an automotive catalytic converter the pressures due to exhaust gases is higher than atmospheric pressure (10^3 mbar), while a model system[2] in a UHV chamber is exposed to not more than 10^{-11} or 10^{-10} mbar. Another difference between the catalytic model systems of surface science and a realistic catalytic system is that the ceramic supports of the catalytically active metal clusters are not single crystals, but they are rough and they have highly complex surface structures with many defects and contaminations.

Although surface science suffers from these unrealistic conditions, which often are described in terms of the "pressure and materials gaps", it has been highly successful in addressing and answering very fundamental questions about how surfaces are organized and work at the atomic scale. For example, surface science has provided very much insight into the relationship between a surface's geometric and electronic structure, into the influence of surface defects on the surface's chemical reactivity, into how materials grow at the atomic scale, into how the adsorption of molecules changes a surface's optical and electronic properties, etc. Nevertheless, the gap is getting smaller by the introduction of new setups capable of performing controlled measurements at higher pressures, new techniques which are compatible with robust conditions, and more realistic materials which can mimic nature better.

Synchrotrons are circular particle accelerators which are constructed for different purposes. Synchrotron radiation facilities (see subsection 2.1.2), which normally are based on electron storage rings, are specifically employed for production of electromagnetic radiation ranging in the infrared to hard X-ray regimes for materials investigations. The main advantages of synchrotron radiation over various other light sources are [2] their (i) high intensity, (ii) broad spectral range, (iii) high

[2] The study of model systems, aimed at demonstrating certain aspects of a complex system, is a typical strategy of surface science. This approach is often called the "surface science approach".

polarization, (iv) pulsed time structure, and (v) high degree of collimation. Synchrotron radiation has applications in a wide range of scientific disciplines with main focuses on spectroscopy, diffraction, and microscopy methods. The introduction of synchrotron radiation facilities made many surface science studies much easier to perform, and in some cases synchrotron radiation facilities were needed to render them feasible to conduct at all. Two of the experimental methods used in this thesis, XPS and XAS, are very good examples in this respect. Photoelectron spectroscopy was developed and successfully used in surface science studies before the construction of the first dedicated synchrotron radiation facilities. However, intense synchrotron radiation with a wide range of available photon energies opened up entirely new possibilities for photoelectron spectroscopy studies. X-ray absorption spectroscopy, for which the variation of photon energy is very beneficial, highly polarized synchrotron radiation made polarization dependent absorption studies feasible.

1.2 Motivation

In this section, three different surface science topics – organic-inorganic interactions, heterogeneous catalysis, and dye-sensitized solar cells – are described briefly. These three subjects are popular and dynamic fields of research and have a variety of applications in technology. The hope is that the connection between this work and the existing knowledge will become clear.

1.2.1 Interactions between Organic and Inorganic Materials

Surfaces are highly significant not only for the physical properties of and chemical processes in solid materials, but also for living organisms and biological systems in general, which all rely heavily on processes at interfaces and surfaces. However, the relationship between surface science and biological systems is still in its infancy. The main reason is the complexity of biological systems. The study of model systems offers a way out since such model systems can mimic certain aspects of their biological counterparts. Therefore, the study of interactions between organic and inorganic substances has become something of a meeting area for biology, materials chemistry, and surface science. During the last decade the investigation of the interactions between organic molecules and inorganic substrates has experienced a substantial upswing. There are many different possible applications and benefits of "biological surface science", a review of which has been given by Bengt Kasemo [3]. Bio-compatibility, bio-functionality, and bio-integration are the new phrases entering the field of surface science.

Materials – metals, ceramics, and polymers – which are implanted into the human body are among the real-life applications of organic-inorganic interfaces. There are certain properties which a candidate implant material should possess, such as the ability of easily getting integrated with the surrounding tissue, zero or extremely low corrosion rates, non-toxicity, strength, and flexibility. Biological surface science can contribute to the improvement of all the listed properties.

Titanium metal and some of its alloys are common implant materials and have been used for dental replacement for a long time [4]. Titanium is a very reactive metal, and in a physiological environment a 3-5 nm (10-15 atomic layers) thick oxide film is rapidly formed at its surface. The stoichiometry of this film is TiO_2-like [5] and found to be dominated by a polycrystalline phase [6].

The oxide film is important as it isolates the metal from the physiological environment and thus prevents metal diffusion into the tissue. Actually, it is the TiO_2 film rather than the pure titanium metal which interacts with the environment and which is responsible for the applicability of the titanium metal as an implant. The chemical compounds in the living organism, such as water, ions and small molecules, lipids, and proteins interact with the surface on different time scales. The water molecules are responsible for the almost instantaneous conversion of the metal surface to a thick oxidized layer. The properties of this oxide surface and adsorbed water layers on top affect the adsorption of other species [7].

The interactions of various different small molecules like O_2, CO, and H_2O with oxide surfaces have been investigated in great detail during the past couple of decades. Less is known about the interaction of larger organic molecules with oxide surfaces. Of particular interest in this context are the natural amino acids, since they are the building blocks of proteins. Answering questions like how amino acids bind to oxide surfaces, what are the intermolecular interactions between adsorbed molecules and molecular orientations, and what is the effect of water molecules on these structures will provide valuable information on how proteins interact with oxide surfaces [3].

1.2.2 Catalysis

Catalysis is defined as the acceleration of a chemical reaction by action of a substance – the catalyst material – which is fully regenerated at the end of the reaction and which does not form part of the stoichiometric equation. Catalysis is commonly found in many natural processes, and it is employed in a large variety of scientific and technological applications, in particular including applications in the chemical industry. Conventionally, catalysis is separated into two categories, namely, homo- and heterogeneous catalysis. In homogeneous catalysis both the reactants and catalyst are in the same phase, while the opposite is true for heterogeneous catalysis.

Improvements in technology have increased the demands on the mass production of new functionalized materials together with a large variety of new chemical compounds. In addition, the growth of human population and our industrialized life-styles brought about many different environmental issues. Mankind destroys the Earth on a day-to-day basis, and this destruction occurs in many different ways. One of the major pathways of environmental destruction is the production of poisonous gases as by-products of combustion of fossil fuels in cars, power plants, and factories.

Under ideal conditions three main gases are produced in the combustion reaction of fossil fuel: water (H_2O), molecular nitrogen (N_2), and carbon dioxide (CO_2). Ideal conditions imply that all fuel is burnt in the process. In the cylinders of a car, combustion is not complete and poisonous gases such as carbon monoxide (CO), nitrogen oxides (NO_x), and non- or only partly combusted hydrocarbons are produced and released from the engine. Heterogeneous catalysis plays a major role in the solution of this environmental problem. During the 1970s researchers found that microscopic, finely dispersed particles of palladium, platinum, and rhodium deposited on a ceramic support simultaneously catalyze the oxidation of CO and the reduction of NO_x and thus substantially reduce the amount of dangerous gases leaving the exhaust of a car [8]. Nowadays, in many countries all over the world there are restrictions for admissible automotive emissions, and all recently produced cars contain a so-called catalytic converter in between the engine and the exhaust, which converts

poisonous gases into less harmful ones. However, there exists a temperature effect, which poses a serious problem: modern catalytic converters become active at around 200 °C only, and measurements show that most of the dangerous gases are emitted in the start-up time of the engine when the converter is cold [9]. Engineers have tried to overcome this problem in two different ways: first, by placing the converters closer to the engine so that gases coming out are warmer and also warm up the converter faster, and second, by warming up the converter with a direct current before starting the engine. Both of these attempts were found to be problematic and therefore inconvenient.

Another possible solution has emerged from the work by Haruta and co-workers [10], who found that Au clusters with certain sizes (<3 nm) supported on different oxides have a high catalytic activity for the oxidation of CO at temperatures lower than room temperature. In general, the mechanism why particles with certain sizes have an increased catalytic activity is still not very well understood, but there are at least four different possible scenarios, which different groups suggest [11]: (i) the activity of the particles is increased at the point where clusters loose their metallic properties, (ii) the clusters are charged when supported by an oxide material, (iii) the interface between the metal particles and oxide support is crucial for the catalytic activity, (iv) clusters contain a high concentration of defects such as kinks and step edges on which the atomic structure is distorted and therefore the activity is increased. A fundamental problem of catalyst materials based on Au clusters supported on TiO_2 is that they sinter and loose their catalytic activity upon increasing the temperature [12] or upon long exposures to oxygen or oxygen/carbon monoxide gas mixtures [13]. At this point it is clear that any external effect which can prevent sintering, such as surface modifications, can keep the efficiency high for longer times. Pre-oxidation of the support material or adsorption of molecular spacers which strongly interacts with the substrate and block the remaining adsorption sites might help to circumvent the sintering problem.

Many support materials – mostly metal oxides – used in catalysis applications and of interest to surface science investigations are not conductive and hence unsuitable for surface science studies based on the detection of electrons. Ultrathin metal oxide films, either produced by oxidation of metal single crystal surfaces or deposited in situ onto various metallic supports, are found to be good model systems, i.e., they are conductive and reproduce some of the bulk oxide properties. However, ultrathin oxide films also have their own novel chemical and physical properties which make them interesting for surface science studies in other aspects.

1.2.3 Dye-Sensitized Solar Cells

The main sources of energy today – mostly fossil-based – will eventually run out and replacements will have to be found. Moreover, as mentioned before, fossil energy is afflicted by the production of many toxic by-products and greenhouse gases such as CO_2. Therefore one of the issues which the world has been facing during the last couple of decades and which will grow even more urgent in the future is the challenge of energy production from renewable, sustainable, and environment friendly resources. Fortunately, there are many other alternative sources for producing energy rather than fossil fuels; e.g. water and wind turbines are among the most common and oldest ones.

Another alternative method of producing energy is by the conversion of sun light into electricity, i.e., by using photovoltaics. The Sun is a very convenient source of energy, since it delivers an amount of

energy to the Earth in one day, which corresponds to the total annual energy consumption of all human activity [14]. However, the production cost and operation efficiency of photovoltaic cells (or solar cells) lags behind that of conventional fossil-based resources.

The idea behind a solar cell is pretty straightforward. An electron-hole pair is created in the solar cell material by the absorption of light. This pair is kept separated, and the electron and hole are transported to different electrodes where they combine. Through the transfer of charges a net electric current is obtained. Conventional solar cell technology is based on solid state devices, in which a junction is formed between differently doped silicon materials. The band gap value of silicon matches the energy of visible light so that, when illuminated, the electrons in the valence band are excited to the conduction band and leave a hole behind. The electron-hole pair is separated by the built-in voltage across the junction. Electrons are transferred to the other side of the junction through the circuit and combine with the holes. The major problem of solid state solar cells is their production costs. Silicon processing is an expensive technology.

The way that dye-sensitized solar cells work is quite different. The light absorption and charge transfer events, both of which occur in the semiconductor material of a conventional solar cell, are separated in a dye-sensitized solar cell [15]. Instead of silicon a mesoporous TiO_2 layer sintered on a conductive glass is used as the semiconductor material. The mesoporous structure makes the surface area of the layer almost three orders of magnitude higher than for a smooth surface and, therefore, the light absorption efficiency is increased greatly [16]. TiO_2 is chosen because it is a robust, cheap, non-toxic, and abundant material, which, however, has a wide band gap and only absorbs ultraviolet light. This issue is circumvented by adsorbing a monolayer of a dye molecule onto the material's surface. By nature, dyes are good at absorbing light in the visible regime, and therefore the TiO_2 is said to be sensitized to the absorption of visible light. The TiO_2-dye system is placed into an electrolyte, which most often is an inorganic solvent composed of an iodide (I^-)/triiodine (I_3^-) redox couple. The cathode is either made of platinum or contains small platinum clusters on its surface, which catalyze the reduction reaction. The photovoltaic process proceeds in the following steps [17]: (i) electrons in the highest occupied molecular orbital (HOMO) of the dye are excited to the lowest unoccupied molecular orbital (LUMO) by absorption of light, (ii) since the energy of the LUMO matches that of the conduction band of the TiO_2 support the excited electrons are transferred to the TiO_2 conduction band and the dye is oxidized, (iii) in the electrolyte $3I^-$ oxidizes to I_3^- and excess electrons reduce the dye molecules back to their original states, (iv) the electrons in the TiO_2 conduction band are transferred to the cathode material through the circuit, (v) the electrons which reach to the cathode are used for the reversed reaction to reduce I_3^- to $3I^-$.

The major drawback of dye-sensitized solar cells is their lower efficiency as compared to that of conventional solar cells. In order to increase the efficiency improvements of dye molecules, electrolytes and interfacial regions are essential [14]. There have been intensive efforts on the fundamental level towards understanding the charge transfer dynamics and chemistry of the semiconductor/dye system and the surface science community has made important contributions to that endeavor. Active research areas of the field are the optimization of strength of the bonds and geometry of dye molecules on semiconductor surface as well as the synthesis and characterization of new dye molecules.

Chapter 2

Methods

In this chapter I will describe the methods used in this thesis. First, I will discuss the physical mechanisms and principles of each method and then practical issues of application and interpretation. My intention is to provide a picture, which is as complete as possible, but at the same time to keep to a level relevant to my work.

2.1 X-Ray Photoelectron Spectroscopy

Photoelectron spectroscopy (PS) is an experimental technique based on the photoelectric effect, which describes the emission of electrons from matter as a result of absorption of photons with sufficient energy. Most often, the name of the technique is extended by adding the designation of the employed photon energy regime, i.e., it is either called Ultraviolet Photoelectron Spectroscopy (UPS) or X-ray Photoelectron Spectroscopy (XPS). This distinction is historical and has little particular significance when a tunable synchrotron radiation source is used in the production of the photons. Basically, in a PS experiment a gas, liquid or solid material is exposed to photons with a well-defined energy and the number of electrons emitted from the material is measured as a function of the electrons' kinetic energy. Therefore, a light source and an electron energy analyzer are the two fundamental components of a PS experimental setup.

The photoelectric effect was first observed by Heinrich Hertz in 1887. The theory of the phenomenon was formulated by Albert Einstein in 1905, who in 1921 received the Nobel Prize in Physics "... for his discovery of the law of the photoelectric effect" [18]. His explanation is based on energy conservation, which imposes that the energy of the light impinging on the material, E_v, should be equal to the kinetic energy of the emitted electron, E_k, plus the energy that is required to extract the electron from the material, $E_b + \phi$, where E_b is the binding energy of the electron and ϕ is the work function of the material. The exact value of the binding energy differs depending on the energy level[3] to which it is referred.

It took some time to realize that the binding energy of an electron in a particular energy level of an element is not only an element-specific property, but that it also depends on the chemical state of the element. In the late 1950s and early 1960s Kai Siegbahn and his co-workers at Uppsala University developed an instrument to measure the kinetic energies of photoelectrons emitted from a specific core level of an element in different chemical environments with sufficient resolution. They were then able to observe *chemical shifts* between the spectral lines, depending on the chemical

[3] Most commonly, for solids the Fermi level and for gases the vacuum level are used as energy references.

environment. Siegbahn received the Nobel Prize in Physics in 1981 “for his contribution to the development of high-resolution electron spectroscopy” [19].

Following the developments of Siegbahn’s group the field started to grow extensively. The development of electron energy analyzers with high energy resolution and of dedicated synchrotron radiation sources were the two main driving forces behind this growth. In time researchers realized how photoelectron spectroscopy can be used to acquire information about the fundamental properties of matter, namely, its electronic, vibrational and rotational structure, and chemical composition and state. The technique is now widely used among physicists, chemists, and material scientists, and it is one of the primary tools of surface science studies.

2.1.1 Theory of X-Ray Photoelectron Spectroscopy

Quantum mechanics, in its simplest form, tackles the photoelectric effect as a time-dependent perturbation problem. The electromagnetic field – the light –, with electric and magnetic fields oscillating in time, changes the Hamiltonian of a system of charged particles in a way that it can be separated into two terms, one of which is assumed to be small and the only time dependent component. This small component, with a suitable choice of gauge for the field, can be simplified in the electric dipole approximation. Fermi’s Golden Rule with the resulting perturbation term can be employed to calculate transition rates and absorption cross sections, photocurrents, or spectral functions.

The Hamiltonian of a system of charged particles isolated from the effect of any external field can be written as

$$H = \sum_k \left(\frac{\vec{p}_k^{\,2}}{2m_k} + V_0\left(\vec{r}_k\right) \right), \tag{2.1}$$

where $\vec{p}_k$ and m_k are the momenta and masses of the individual particles, respectively. V_0 is the internal potential which holds together the system. The summation runs over all particles. When the system interacts with an external electromagnetic field, classical theory shows that the Hamiltonian changes to [20]

$$H = \sum_k \left[\frac{1}{2m_k}\left(\vec{p}_k - q_k\vec{A}\left(\vec{r}_k\right)\right)^2 + q_k\phi\left(\vec{r}_k\right) + V_0\left(\vec{r}_k\right) \right], \tag{2.2}$$

where $\vec{A}$ and ϕ are the vector and scalar potentials representing the external electromagnetic field, and the q_k are the charges of the particles. If one writes explicitly the squared term in parentheses, treats the momentum operator quantum mechanically ($\vec{p} = -i\hbar\vec{\nabla}$), neglects the $\vec{A}^2$ term, and uses the Coulomb gauge ($\phi = 0$ and $\vec{\nabla}\vec{A} = 0$), then the Hamiltonian can be separated into two components:

$$H = H_0 + \sum_k \frac{q_k}{m_k}\vec{A}\left(\vec{r}_k\right)\vec{p}_k\,. \tag{2.3}$$

The way the Hamiltonian is written in Equation (2.2) and the derivation of Equation (2.3) is called the *semi-classical approach*, since in this way the light is not treated quantum mechanically – which means it is not represented by photons – while the particle momenta *are* treated as quantum mechanical operators. The $\vec{A}^2$ term can be neglected in the low light intensity regime, i.e., for two-photon interactions. It is also important to realize that the spin of the particles does not enter the story at all. In the way that the transition probability will be written it can be shown that the coupling of the spin with electromagnetic field can also be neglected [21].

The second term in Equation (2.3) is the one which is time-dependent and responsible for the transition of the system from an initial state ψ_i to a final state ψ_f. It can be shown that the electromagnetic waves can be represented by plane waves, and by using the electric dipole approximation the expression for perturbation term can be simplified further. Since the perturbation is periodic in time, Fermi's Golden Rule can be employed to calculate the transition rate as [21]

$$w_{i\to f} = \frac{2\pi}{\hbar^3} E_0^2 \frac{\left(E_f - E_i\right)^2}{\omega^2} \left| \left\langle \psi_f \left| \hat{\varepsilon} \cdot \left(\sum_k q_k \vec{r}_k \right) \right| \psi_i \right\rangle \right|^2 \delta\left(E_f - E_i - \hbar\omega\right), \tag{2.4}$$

where E_0 is the intensity of the electric field of the light and $\hat{\varepsilon}$ is the unit vector in the direction of the electric field (i.e., it represents the direction of polarization of light). E_f, E_i, and $\hbar\omega$ are the energies of the final and initial states of the system and light, respectively. The δ function takes care of the energy conservation in the transition. The $\sum q\vec{r}$ operator in the matrix elements is the dipole operator, which is responsible for the transition and determines the selection rules. Thus, the problem of calculating the transition rate is reduced to the problem of calculating the dipole matrix elements.

In the case of photoemission from a core level (in an atom, molecule, or solid) an electron, which is initially bound to the system, absorbs a photon and is excited to the continuum with a certain kinetic energy. To be able to write the wave functions for the initial and final states one can use the *one-(independent) electron approximation*, which states that the wave function of a system of electrons can be written as an antisymmetrized sum of products of one-electron wave functions (Hartree-Fock method). If we assume that the system initially has N electrons, one of which is photoemitted from a level c (for core level), then the matrix elements can be written as [22]

$$\left\langle \psi_f \left| \vec{r} \right| \psi_i \right\rangle = \left\langle \phi_{f,E} \left| \vec{r} \right| \phi_{i,c} \right\rangle \left\langle \psi_{f,R}^c \left(N-1\right) \middle| \psi_{i,R}^c \left(N-1\right) \right\rangle, \tag{2.5}$$

where $\phi_{i,c}$ and $\phi_{f,E}$ are the wave functions of the photoemitted electron before and after emission (with kinetic energy E) and where, correspondingly, $\psi_{i,R}^c\left(N-1\right)$ and $\psi_{f,R}^c\left(N-1\right)$ are the wave functions of the remaining (R) electrons before and after emission, respectively. In the *frozen orbital approximation* one assumes that the remaining electrons are not affected by the photoemission process so that their wave functions do not change, and the second term on the right hand side of Equation (2.5) becomes unity. In such an unrealistic case XPS measures the Hartree-Fock orbital energy, the negative of which is also called Koopmans' binding energy [23]. In reality, as soon as the core hole is created by the emission of an electron, the remaining electrons readjust themselves so that the final state wave function is changed. This phenomenon is called relaxation and creates the so-called shape-up/shake-off satellite structures in the photoemission spectra.

A couple of significant approximations have been made to reach Equations (2.4) and (2.5), and of course there are certain limitations for their validity. Nevertheless, the most important point to realize is that photoemission is a quantum mechanical transition of a system from an initial state to a final state, and that this transition is driven by the dipole operator. In principle this means that the binding energy of a photoemitted core electron is sensitive to the initial *and* final states of the system under consideration. It is common practice to attribute the observed changes (shifts) in binding energies to initial and/or final states effects. The initial state of a system depends on the chemical state and the environment of the atom from which the photoelectron is emitted. This is true in spite of the fact that the core levels are quite localized around the nuclei and do not participate in bonding. For example, binding energy shifts which are observed for different oxidation states, surface and bulk atoms of a solid material[4], different types of bonding, and number and identity of bonding atoms are generally regarded as initial state effects. The final state effects take place after excitation of the system. For example, relaxation of the remaining electrons in the excited atom (intra-atomic screening) as a response to the creation of a core hole, the satellites resulting from the excitation of valence electrons to upper bound or unbound states and creation of plasmon oscillations in the material (metals) can be considered as final state effects. Another commonly observed final state effect occurs when the atom from which the electron is emitted is inside or adsorbed on a solid material. In this case electrons of the material react to the creation of the core hole to screen its charge (extra-atomic screening) and lower the final state energy of the system.

A theoretical framework to understand how initial and final state effects produce core level binding energy shifts (ΔE_B) is based on the one-electron approximation. In this framework the shift are given by [23]

$$\Delta E_B = \Delta\varepsilon + \Delta E_R + \Delta E_C . \qquad (2.6)$$

$\Delta\varepsilon$ is the difference in orbital energy (Koopmans' binding energy) between the species for which a spectral shift observed and represents the initial state effects, ΔE_R is the difference in relaxation energy (intra- or extra-atomic screening) and represents the final state effects, and ΔE_C is the difference in electron correlation energy, which is usually assumed to be the same in the same system and therefore neglected. It should be strongly emphasized that the interpretation of binding energy shifts as in Equation (2.6) is a fully theoretical concept and has the potential of leading to wrong conclusions if not employed with caution. Nevertheless, in some of the cases it is applied to explain experimental results with reasonable or even good agreement [24].

The above paragraphs describe the theory of XPS on a level relevant to the present work. There are more elaborate approaches to photoemission (see, for example Ref. [25]), which in practice would bring nothing new to the understanding of the work done here.

[4]In some cases it is found that initial state considerations only can not explain the observed surface core level shifts and final state effects should be taken into account.

2.1.2 Instrumentation and Experimental Aspects of X-ray Photoelectron Spectroscopy

As mentioned before, a photoelectron spectroscopy setup consists of two main components, the light source and the electron energy analyzer. The purpose of this section is to briefly describe the equipment used in XPS measurements and provide some practical information on how to operate it.

Two different types of light sources exist for XPS measurements, lab-sources (X-ray tubes) and synchrotron radiation sources. An X-ray tube basically consists of an anode and an electron gun. The electrons produced by the gun are accelerated towards the anode and kick out the electrons from different energy levels of the material. The excited atoms relax mainly by X-ray emission. In some of the instruments the emitted X-rays are passed through a monochromator, which not only filters away undesired wavelengths, but also focuses the light onto the sample. There are different characteristic emission energies for different materials. The most commonly used transitions are the Al and Mg K_α lines, which produce photons with an energy of 1486.6 and 1253.6 eV, respectively. The advantages of X-ray tubes are that they are relatively cheap and easily accessible; on the other hand the fixed photon energy and low energy resolution are the major drawbacks.

Synchrotron radiation is produced in a totally different way. The fundamental principle is the creation of electromagnetic radiation through acceleration of charged particles. Electrons circulating at nearly the speed of light in a storage ring are accelerated in terms of deflections from their straight trajectories to produce synchrotron radiation. The ring is kept at UHV to minimize the loss of electrons by residual gas scattering. Magnetic fields are used to keep the electrons on the desired trajectory. The energy spent for the emission of light is replenished by radio frequency (RF) cavities in each cycle. RF cavities accelerate electrons through oscillating electric fields inside a copper block. This way of acceleration causes the electrons to accumulate together in bunches. Relativistic electrons, which are accelerated sideways, emit electromagnetic radiation into the forward direction, and therefore beamlines are built into the emission direction. Before entering into the experimental end station, the light is monochromatized and focused through the beamline. Most commonly, gratings are used for monochromatization and focusing is achieved by series of mirrors in different shapes and orientations. In Figure 2.1 a schematic drawing of a simplified storage ring with a single beamline is shown.

There are three main advantages of synchrotron light sources relevant to XPS measurements reported in this work: the tunability of the photon energy, high intensity, and high photon energy resolution. However, synchrotron radiation facilities are expensive to build and maintain, and usually the schedules are overloaded. The time slots one gets for an experiment (beamtimes) can be quite tiring and challenging in many aspects.

The early use of synchrotron radiation was more like a shark-suckerfish relation between high energy physicists and synchrotron radiation researchers who had to parasitically use synchrotrons (first generation) built to accelerate particles for high energy collisions. The usage of synchrotrons for the purposes of high energy physics was not the optimum condition for synchrotron radiation work. The first dedicated storage ring for the production of synchrotron radiation (second generation) was built in the USA in 1968 [2]. The greatest development in the field was the invention of so-called insertion

devices (third generation) to enhance the light intensity. Insertion devices (wigglers and undulators) are series of alternating poles of magnets which are placed on the straight sections of the storage rings (cf. Figure 2.1). Electrons enter from one side of this array of magnets and follow a sinusoidal trajectory inside. As a result intense and collimated light is produced on the other side of the insertion device.

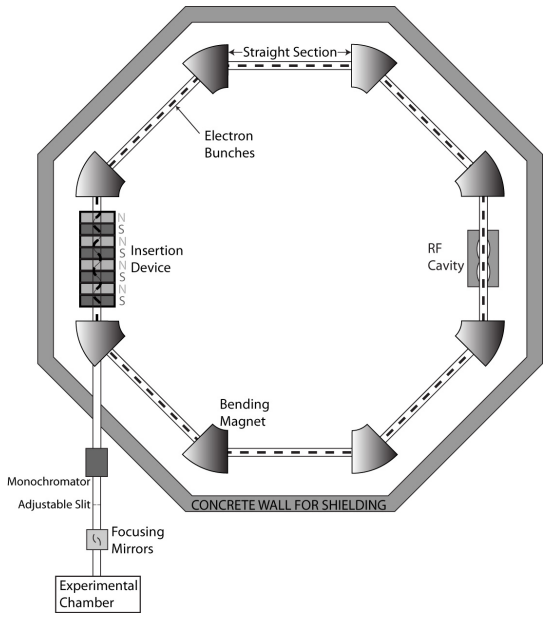

Figure 2.1 A schematic drawing of a storage ring and a beamline, which are separated from each other by a concrete wall. Electrons inside the ring circulate close to the speed of light and emit electromagnetic radiation whenever they are accelerated by means of deflections from the straight trajectory. The lost energy is replenished in the radio frequency (RF) cavity in each turn. The way the RF cavity works forces electrons to accumulate in small bunches. An insertion device is introduced on a straight section of the ring to create high intensity light which is monochromatized and focused into an experimental end station.

Electron energy analyzers are the instruments which are used to measure the intensity of the photoemitted electrons as a function of the electrons' kinetic energy. There are different types of electron energy analyzers developed and used for different purposes. Here, emphasis will be on the particular type of analyzer which is used in the measurements presented in this thesis, namely the hemispherical electron energy analyzer or concentric hemispherical analyzer (CHA). A schematic drawing of a CHA and a photoemission experiment is given in Figure 2.2. As light hits the sample photoelectrons are emitted in all directions. A fraction of the photoelectrons (light gray arrows in Figure 2.2) will be captured by the analyzer as determined by the acceptance angle of the instrument. The electrons with sufficient energy enter the analyzer and they are either accelerated or retarded to a certain energy (the pass energy) by an electrostatic lens system, which also focuses the electron beam onto the entrance slit (light gray area in Figure 2.2). At the end of the lens assembly the electrons are spatially filtered by an adjustable slit before entering the hemispheres. The inner and outer spheres are kept at constant positive and negative voltages, respectively. The electric field created in between the spheres bends the electron trajectory and leads the electrons to a microchannel plate (MCP). The electrons which have more (faster) or less (slower) energy than a certain value (approximately the pass energy) hit the outer or inner spheres, respectively and can not reach the MCP. Therefore, the electrons which reach the MCP have a known energy. On the MCP they create cascades of secondary electrons, which afterwards are accelerated towards a phosphor screen where they create

bright spots. The intensity of the bright spots on the phosphor screen is registered by a charged-coupled device (CCD) camera and is proportional to the intensity of electrons with that particular energy. By keeping the pass energy constant and sweeping the acceleration or retardation voltage in the lens system, the intensity of electrons as function of kinetic energies can be measured.

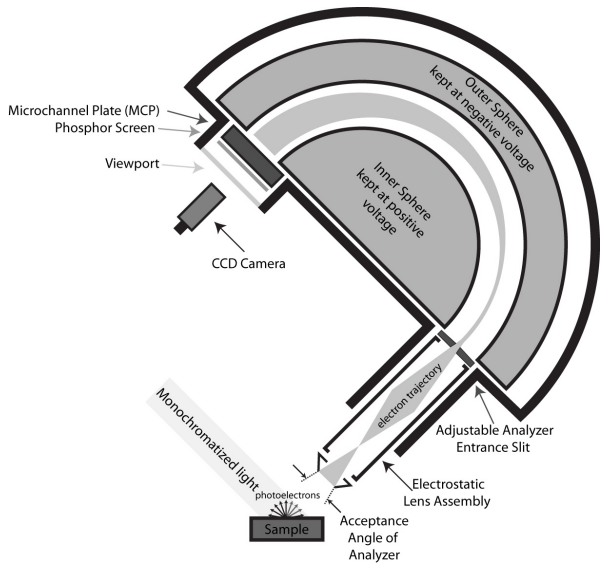

Figure 2.2 A schematic drawing of a hemispherical electron energy analyzer and a photoemission experiment. Monochromatized light impinging on the sample creates photoelectrons in every direction. Only some of them can enter the analyzer. An electrostatic lens system retards/accelerates the electrons to a certain value of energy (E_p) and focuses them onto the entrance slit. Electrons with energy E_p can pass through the gap between the hemispheres and detected by a microchannel plate detector. The intensity is measured by a phosphor screen and a CCD camera.

As shown in Figure 2.2 the electron beam is expanded inside the analyzer from the entrance slit to the MCP. This is due to the finite gap size between the inner and outer hemispheres. Even for an infinitesimally small entrance slit, the electrons which have a little higher or lower energy than the pass energy can go through the gap of the analyzer and reach different parts of the MCP. Lowering the pass energy will give a narrower energy window to electrons of different energies to reach the MCP and increase the energy resolution. In practice the entrance slit of the analyzer has a finite value which lets an electron beam with wider angular distribution pass through. This will increase the possibility of electrons with different energies to reach the same spot on the MCP through different paths inside the gap; hence opening up the entrance slit lowers the energy resolution. Smaller slits and lower pass energies should, therefore, be used to reach higher energy resolution. However, increasing the resolution in this way reduces the number of electrons which reach the MCP and cause lower count rates. The best way to overcome this problem is to create as many photoelectrons as possible. The only way to increase the number of photoelectrons emitted for a particular energy level of an element is to increase the number of photons impinging on the material. This is one of the reasons why the availability of high intensity synchrotron radiation sources has affected the field in such a substantial way.

The quality of a photoelectron spectrum is determined by a high signal-to-noise ratio and high energy resolution. The resolution can be improved by either improving the resolution of the light source or of the analyzer as described in above paragraph. The signal-to-noise ratio increases with higher electron count rates, which in turn can be increased by a longer counting time, higher photon

flux, or higher analyzer transmission. What made Siegbahn's group more successful than the others and what earned him the Nobel Prize was the resolution they achieved. He concluded this in the following sentence: "I realized that electron spectroscopy for atoms and solids could never become competitive with X-ray emission or absorption spectroscopy unless I was able to achieve such a high resolution that really well-defined electron lines were obtained with linewidths equal to or close to the inherent atomic levels themselves" [26].

An important point to mention is that XPS is a surface sensitive technique. X-ray photons, as used in XPS, can penetrate approximately a couple of microns into the material. However, this is not the case for electrons. As mentioned in section 1.1, the inelastic mean free path[5] (IMFP) of electrons, which is a measure of how long distance an electron can travel inside a material without suffering an inelastic scattering, is relatively small. Even though the IMFP is a material-dependent property (or, rather, it depends on the dielectric constant) the IMFP's dependence on kinetic energy of the electrons is similar in different materials. This fact is usually represented by the so-called universal curve for the IMFPs of electrons. In particular, electrons with kinetic energies in between ~50-100 eV have minimum IMFP values of ~5-10 Å. Only the photoelectrons emitted from the first couple of layers of the surface of a sample can reach the analyzer without loosing energy.

2.1.3 Interpretation and Analysis of Core-Level Photoelectron Spectra

XPS is one of the experimental techniques which for a conductive sample always give a result. The challenging issue for the experimentalists is to make sure that what is measured is what should have been measured, to attribute correct meanings to the observed spectra and their individual components, and to reach the conclusions that in the best case can be supported by other experimental or theoretical methods.

The values of core-level binding energy shifts, which are observed in XPS measurements, typically range from tens of millielectron volts to a couple of electron volts. The smallness of the core-level binding energy shifts, when considered together with the finite experimental energy resolution and the line broadening effects, reveals that X-ray photoelectron spectra often are composed from overlapping components (peaks). Therefore, in many cases curve fitting is an essential task in a reliable analysis of X-ray photoelectron spectra. There are five important questions which should be answered when dealing with an x-ray photoelectron spectrum [28]: (i) What is the shape of the background? (ii) How many peaks should be used? (iii) What is the line shape of the peaks? (iv) What is the width of the peaks? (v) What is the degree of asymmetry? In the following paragraphs a general approach to these questions are presented.

When a solid material is exposed to light electrons, with binding energies lower than the energy of the impinging light, are photoemitted with a certain probability. Upon photoionization – and emission into the vacuum – some of the photoelectrons may reach the analyzer without losing their energy and a photoemission peak at a characteristic binding energy is observed. Many more excited electrons lose energy and contribute to a background signal at kinetic energies below that of the

[5] In fact, a better quantity as a measure for surface sensitivity is the mean escape depth which is defined as "the average depth normal to the surface from which the specified particles or radiation escape" [27].

characteristic peak. The background emerges at the characteristic binding energy, and the increase often has a step-like appearance. The largest contribution to the background is featureless, but there also occur features at well-defined energies, both due to intrinsic and extrinsic losses. The intrinsic losses are related to the photoemission process as described in the *three-step model* [6] of photoemission, while the extrinsic losses are attributed to scattering during the transport of the photoelectrons to the surface and emission into the vacuum [22]. One normally wants to remove the featureless background from the spectra. However, background removal is a non-trivial problem, since the exact shape of the background is very difficult to determine. There exist different advanced models but in this work only very simple, rather phenomenological models have been used such as polynomial and Shirley backgrounds [29].

The number of the peaks and their relative intensities are in principle determined by the stoichiometry of the sample. As discussed above it is expected that the binding energies of the electrons in the same energy level of an atom depend on the chemical environment. Nevertheless, since both initial and final states effects contribute to the observed binding energy, different species may have the same or very similar binding energies, and the corresponding components might be difficult to resolve experimentally. Furthermore, inelastic scattering losses and/or photoelectron diffraction effects may cause deviations from the expected intensities. Unfortunately, there is no simple way to determine the exact binding energy values or relative intensities. The two most common approaches are: either to aim for an agreement with well established literature values or to take the intensities as they are.

Once the background is removed from a spectrum the components in the remaining signal can be modeled using different line shapes. There are two main line shape broadening mechanisms, namely, broadening due to the finite resolution of the instrument, which is represented by a Gaussian curve, and broadening due to the limited lifetime of core hole, which is described by a Lorentzian curve. The expected line shape is a convolution of these two curves, i.e., a Voigt line shape. The total instrumental resolution – described by the width of the Gaussian curve – is determined by the energy resolutions of the light source and analyzer. The core hole lifetime – which is mirrored by the width of the Lorentzian curve – is an element- and energy level-specific property, which is not affected significantly by the chemical environment of the atom [30] and tabulated values can be found in literature [31]. In addition to these two fundamental line shape broadening mechanisms also in particular vibrational broadening plays a very important role and is represented by a Gaussian curve, since, generally, the individual vibrational components are not resolved.

In metals, different final states can be populated with small differences in energy due to the availability of conduction band levels directly above the Fermi level. This results in an asymmetry of the core-level photoemission line on the high binding energy side. Often, the line can then be described by a Doniach-Šunjić line shape [32]. For semiconductors, as investigated in this thesis, the Doniach-Šunjić line shape is not applicable since they have a gap in the electronic levels above the Fermi level. Therefore, in the modeling of spectra obtained on semiconductors symmetric Voigt profiles have been used.

[6] In the model the photoemission process is broken up into three sub-processes: (i) excitation of the electron, (ii) transfer of the photoelectron to the surface, and (iii) emission of the photoelectron into the vacuum.

2.2 X-ray Absorption Spectroscopy

X-ray absorption spectroscopy (XAS) is the measurement of absorption coefficient as a function of X-ray energy. An X-ray absorption spectrum was observed for the first time by Maurice de Broglie in 1913. This spectrum was later correctly interpreted as the K adsorption edges of silver and bromine [33]. An absorption edge is a step-like rise in the spectrum as a result of a transition from an inner shell energy level (K or L) to a bound or free unoccupied level induced by the absorption of an X-ray photon. The position of an absorption edge contains information about both the chemical species present, since every element has well-defined inner shell energy levels, and the oxidation state. However, nowadays XAS is hardly ever used only for elemental identification since the oscillatory "fine" structure observed in spectra up to several hundred eV above an absorption edge contains much more information.

There are different conventions for the naming of the energy regions in an X-ray absorption spectrum and likewise, the information content varies with energy. The region from the absorption edge up to approximately 40 eV is called X-ray absorption near edge structure (XANES) or near edge x-ray absorption fine structure (NEXAFS), and the region from the upper boundary of the NEXAFS region a couple of hundreds eV upwards is called the extended X-ray absorption fine structure (EXAFS) region. Together they are referred to as X-ray absorption fine structure (XAFS) or XAS. In the following subsections the NEXAFS region which is used to for the work of this thesis is discussed.

2.2.1 Theory of Near Edge X-Ray Absorption Fine Structure

The physical principle which is exploited in XAS is not different from the one in XPS. Both of the processes are just different aspects of the same phenomenon, namely, the interaction of electromagnetic radiation with matter. In XPS the kinetic energies of electrons, which make transitions from bound states to the continuum, are measured and therefore the occupied states are probed. In contrast, in NEXAFS spectroscopy the absorption of photons, which cause transitions of bound electrons to unoccupied states in the vicinity of the ionization threshold, is measured and therefore the unoccupied states are probed. In both cases the transition is driven by absorption of an X-ray photon by a core electron. For the calculation of transition rates and related quantities in XAS time-dependent perturbation theory through Fermi's Golden Rule can be employed and the dipole approximation is valid as in the case of XPS (see subsection 2.1.1).

The particular strength of NEXAFS spectroscopy is the possibility of extracting information about the orientation of adsorbed molecules relative to the polarization of the light, which in turn is defined with respect to the studied surface. X-ray absorption is measured for different angles between the direction of polarization of light and the surface. The dependence of the absorption coefficient on the incidence angle can be derived for a simplified case. For a linearly polarized light the transition rate for absorption process in the dipole approximation can be written as [34]

$$w_{i\to f} \propto \left|\left\langle \psi_f \left| \hat{\varepsilon}\cdot\vec{r} \right| \psi_i \right\rangle\right|^2 \propto \left|\hat{\varepsilon}\cdot\left\langle \psi_f \left| \vec{r} \right| \psi_i \right\rangle\right|^2, \tag{2.7}$$

where $\hat{\varepsilon}$ and $\vec{r}$ are unit vectors in the direction of light polarization and position vector of the charged particles in the system, respectively. In NEXAFS studies the interest is mostly in K shell absorption of elements with low atomic numbers, such as C, N, and O. Therefore, the initial and final state wave functions can be written in spherical coordinates as

$$\begin{aligned} |\psi_i\rangle &= |1s\rangle = R_{1s}(r), \\ |\psi_f\rangle &= a|2s\rangle + b|2p_x\rangle + c|2p_y\rangle + d|2p_z\rangle \\ &= aR_{2s}(r) + R_{2p}(r)\left(b\sin\theta\cos\phi + c\sin\theta\sin\phi + d\cos\theta\right), \end{aligned} \tag{2.8}$$

where R(r) is a radial wave function, and the final state wave function is written as a linear combination of atomic orbitals. Putting the wave functions into the matrix element in Equation (2.7) gives

$$\langle\psi_f|\vec{r}|\psi_i\rangle = \vec{O}\frac{4\pi}{3}\int R_{1s}(r)R_{2p}(r)r^3dr, \tag{2.9}$$

where $\vec{O} = b\hat{i} + c\hat{j} + d\hat{k}$ is a vector in the direction of the largest amplitude of the final state molecular orbital, and $\hat{i}$, $\hat{j}$, and $\hat{k}$ are unit vectors of a suitable Cartesian coordinate system with the z-axis chosen parallel to the surface normal. The transition rate can then be calculated as

$$w_{i\to f} \propto \left|\langle\psi_f|\hat{\varepsilon}\cdot\vec{r}|\psi_i\rangle\right|^2 \propto \left|\hat{\varepsilon}\cdot\vec{O}\right|^2 \propto \cos^2\delta, \tag{2.10}$$

where δ is the angle between $\hat{\varepsilon}$ and $\vec{O}$.

In Figure 2.3 the situation described by Equation (2.10) is presented schematically. A diatomic molecule is assumed to be adsorbed on a substrate parallel to the surface. Two different orbitals, which are perpendicular to each other, are represented by the $\vec{O}$ and $\vec{O}'$ vectors. Linearly polarized light impinging on to the material is represented by a wavy line; the polarization direction is given by $\hat{\varepsilon}$. On the right-hand side the corresponding absorption spectra are shown. It is assumed that the orbitals represented by $\vec{O}'$ and $\vec{O}$ vectors are the lowest unoccupied molecular orbital (LUMO) and the LUMO+1, respectively. The most (least) intense absorption occurs when the light polarization vector is parallel (perpendicular) to the orbital direction. What is described by Equation (2.10) and shown in Figure 2.3 is the essence of NEXAFS spectroscopy in the determination of orientation of molecules adsorbed on surfaces.

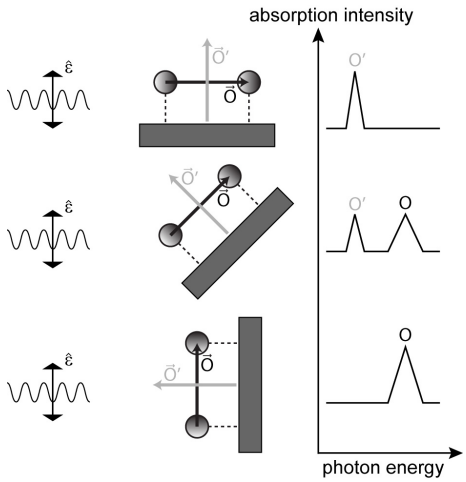

Figure 2.3 Schematic representation of a NEXAFS measurement for a diatomic molecule adsorbed on a substrate. The light impinging on the substrate is represented by a wavy line. The direction of the polarization of the light is given by $\hat{\varepsilon}$. The directions of largest amplitudes of the LUMO and LUMO+1 are represented by $\vec{O}'$ and $\vec{O}$ vectors, respectively. On the right-hand side absorption spectra for three different angles (corresponding to the cases on the left) are depicted.

2.2.2 Measurement and Interpretation of Near Edge X-Ray Absorption Fine Structure

Measurement of an X-ray absorption spectrum can be carried out (i) in a direct way by measuring the intensities of incident, scattered, and transmitted X-rays or (ii) in an indirect way by measuring the products of the decay process of the core hole which is created by photon absorption. Different measurement techniques are employed for different purposes. For example, for liquids the direct method is practical, since incident, transmitted, and scattered X-rays can be measured easily. For solids, however, the direct method is impractical due to the fact that X-rays with energies in the region of interest can not penetrate deeply into solid materials and that therefore the transmitted intensity is zero. Even for thin materials for which X-rays can pass through the sample the spectra would be dominated by bulk signal. Therefore, normally indirect methods are preferred in surface studies.

The core hole created in the X-ray absorption process can decay in two different ways, namely, through emission of photons (X-ray fluorescence) or through emission of electrons (Auger process). For surface science studies measurements are most often performed by monitoring the electron emission process, i.e., the measurements are performed in electron-yield mode. The reasons are that, on the one hand, the low electron IMFP ensures surface sensitivity and, on the other hand, for decay of K shell core holes of elements with low atomic number elements the rate of Auger process is almost 100% [35].

Electron yield measurements can be performed in various ways. In Auger electron yield (AEY) mode the intensity of the Auger decay is monitored. For this purpose electron energy analyzers used for XPS measurements can be employed. In an AEY measurement the analyzer energy window is fixed to a certain kinetic energy region, at which the specific Auger electrons are found. The photon energy is scanned, and the electron count is recorded as a function of the photon energy and kinetic energy. Integrating the intensity for each value of the photon energy yields the XAS spectrum. The other two electron yield methods, the total and partial electron yield modes, are only slightly different. In total electron yield (TEY) mode all electrons emitted from the surface are measured. This way of measuring an absorption spectrum is not particularly surface sensitive, since the secondary electrons in the secondary tail of the X-ray photoelectron spectrum have suffered from multiple scattering events, which is more likely if the electrons' origin is deeper inside the sample. The secondary electrons can be avoided by employing the partial electron yield (PEY) mode, in which a negative bias is applied to the instrument and thus the low-kinetic energy electrons are filtered away from the measurement and the surface sensitivity is increased. Still, the Auger electron yield mode is most surface sensitive since the contribution of inelastically scattered electrons is small.

In a NEXAFS spectrum one observes the transitions of K shell electrons into unoccupied π^* or σ^* molecular orbitals. If π bonds are present, the lowest unoccupied molecular orbital is usually a π^* orbital, and therefore the first (lowest energy) resonance is a π^* resonance. Quite generally, the π^* resonance are found below the ionization threshold, and, compared to the corresponding levels in the absence of the core-hole[7] they typically have a lower energy due to the Coulomb interaction between the hole and excited electron. In contrast, σ^* molecular orbitals are generally found above the ionization threshold. Both the π^* and σ^* resonances have distinct line shapes. π^* resonances are observed as sharp peaks because of their lifetime, which is long because the states can decay only by filling of the core hole with a valence electron (including the excited electron). σ^* resonances are wider and have an asymmetric shape towards higher photon energies. The width and asymmetry of the peak are a result of the coupling of the excited state to continuum states (by tunneling of the excited electron), which significantly shortens the lifetime of the particular excited state. Further asymmetry – for both the π^* and σ^* resonance – results from vibrational motion of the molecule [36].

Orbitals in a molecule have well defined directions which are determined by the atomic structure of the molecule. These distinct geometrical properties, and therefore the orientation of a molecule on a surface, can be probed by changing the orientation of the linear polarization of the light. For example, the diatomic molecule which is showed in Figure 2.3 could be N_2 or CO, and the $\vec{O}$ and $\vec{O}'$ vectors could represent the σ^* and π^* orbitals, respectively. In this way, the set of measurements shown in Figure 2.3 would be enough to determine the adsorption geometry of the molecule on the surface.

There are a couple of practical issues related to the measurement of NEXAFS spectra. The first issue is the strong variation of the photon flux with photon energy. The light is passed through a monochromator and a number of other optical elements in the beamline before it reaches the sample. Absorption of light on these optical elements may vary strongly with photon energy, e.g., especially in the C K-edge region, and the flux will be modulated accordingly. Likewise, the storage ring will emit a certain spectrum with a non-constant photon flux. In the worst case, also instabilities in the

[7] These can be assessed using Inverse photoemission spectroscopy or calculations.

storage ring current may affect the photon flux. Therefore, the NEXAFS raw data are always normalized to the photon energy-dependent photon flux. There exist different ways of achieving this, the most common of which is the measurement of the photon flux on a metallic mesh in front of the experimental chamber or the determination of the beamline transmission by a photodiode. The second issue is the exact determination of photon energy. One of the most exact methods is to measure the energy difference between first- and second-order light coming out from monochromator.

2.3 Scanning Tunneling Microscopy

Scanning tunneling microscopy (STM) is one of the most widely used experimental techniques in surface science and nanotechnology laboratories all over the world for imaging surfaces and interfaces with atomic resolution. It is not only this superior resolution of STM for imaging which makes it so popular, but also its applicability in a wide range of conditions, i.e., at different pressures and temperatures. The major drawback of STM is that, in the case of solids, it only works for conductive materials (metals or sufficiently conductive semiconductors).

STM was invented[8] at the IBM Zurich Research Laboratory by G. Binnig and H. Rohrer in 1982 [37,38]. They published early experimental results in 1982 [39] and 1983 [40]. In the latter paper they were able to explain one of the most complicated surface reconstructions known, the (7x7) reconstruction of the Si(111) surface. G. Binnig and H. Rohrer were awarded the Nobel Prize in Physics in 1986 “for their design of the scanning tunneling microscope” [41].

The basic idea behind STM is pretty straightforward. An atomically sharp metallic tip, often made of tungsten or a platinum-iridium alloy, is kept at a couple of Ångströms away from the sample surface, and a bias voltage is applied between the tip and surface. Although the tip and sample are not in mechanical contact, a net flow of electrons can be achieved either from the sample to tip or from the tip to sample depending on the polarity of the bias voltage. Actually, there are always some electrons moving back and forth in between the tip and sample, but the net current is zero as soon as the bias voltage is off. The basic quantum mechanical phenomenon behind this effect is quantum tunneling through a potential barrier. Many different parameters determine the exact conductivity of the system, but, roughly, bias voltages in the millivolt or volt ranges can result in tunneling currents in the pico- or nanoampere ranges. For imaging a certain region the tip is scanned over the surface with high positioning accuracy with the help of piezoelectric materials. Either the tunneling current is recoded, while the position of the tip in the direction of surface normal is fixed (constant height mode), or – more commonly – the movement of the tip is recorded, while the tunneling current is kept constant (constant current mode). In these ways 3D images of the surfaces are produced.

[8] As all other scientific and technological breakthroughs the invention of STM was also based on the works of others, see [37] for a review of the historical development.

2.3.1 Theory of Scanning Tunneling Microscopy

Early theoretical treatments of electron tunneling in quantum mechanical systems, undertaken to understand the alpha decay and field emission, are almost as old as Schrödinger's discovery of wave mechanics. There are two different main approaches to the description of tunneling, one as a time-dependent initial-value problem (called transfer the Hamiltonian method after Oppenheimer) and the other as a stationary state problem. In the stationary state approach the quantum states in the continuum are treated as weakly quantized levels. An exact one-electron Hamiltonian is used to calculate the tunneling current flow and often the WKB (Wentzel–Kramers–Brillouin) approximation is employed to calculate the transition probabilities. In the time-dependent approach the system is initially defined as localized on one side of the barrier. The Hamiltonian of the entire system is split up into three different components and one of them (the transfer Hamiltonian) is treated as a perturbation term. Electrons which are initially localized on one side have a chance to leak through the barrier to the other side as soon as the perturbation is switched on [42].

In the case of STM tunneling conventionally the time-dependent approach is taken to derive an expression for the tunneling current. The starting point is to use Fermi's Golden Rule to calculate the transition rate between tip and sample states. The matrix elements in Fermi's formula are approximated by Bardeen's approach. By taking the occupation probabilities of different states into account, the transition rate gives the current when multiplied by the charge of the electron.

Two decades before the invention of STM, one of the fathers of the theory of superconductivity, J. Bardeen, published a theoretical description of tunneling from a many-particle point of view (which was based on the time-depended approach) to be able to explain the experimental results on tunneling between two metallic materials separated by a thin oxide layer [43]. In this paper, to define the transition rate of an electron between two different states of metals at each side of an oxide layer through which the electrons tunnel, Fermi's Golden Rule is employed as[9]

$$w_{\mu\to\nu} = \frac{2\pi}{\hbar}\left|M_{\mu\nu}\right|^2 \rho_\nu , \tag{2.11}$$

where $w_{\mu\to\nu}$ is the transition rate between tip states μ of energy E_μ to sample states ν of energy E_ν. $M_{\mu\nu}$ is the transition matrix element and ρ_ν is the density of sample states (number of states per unit energy around ν which is approximated to $\delta\left(E_\mu - E_\nu\right)$ for elastic tunneling). Bardeen split the Hamiltonian of the entire system up into two different Hamiltonians (tip and sample) into which the barrier potential is incorporated and showed that the matrix element $M_{\mu\nu}$ can be written as

$$M_{\mu\nu} = -\frac{\hbar^2}{2m}\int\left(\chi_\nu^*\vec{\nabla}\psi_\mu - \psi_\mu\vec{\nabla}\chi_\nu^*\right)\cdot d\vec{S}, \tag{2.12}$$

where m is the mass of electron, χ_ν and ψ_μ the wave functions of sample and tip states, respectively, and $\vec{S}$ is any surface in the barrier region separating the tip and sample and directed towards the tip. Equation (2.12) has no dependence on energy so that the transition rate is only a function of the

[9] A different version of Bardeen's theory which is transformed to fit to the case of STM tunneling is given here.

density of final states. The derivation of Equation (2.12) is not straightforward and detailed studies can be found in literature [44,45].

Once the matrix elements are represented as in Equation (2.12), the only thing needed for the calculation is to find out the wave functions and plug them into the integral on the right hand side of the equation. Tersoff and Hamann were the first who approximated the tip wave functions as radially symmetrical waves (*s*-waves) and considered the surface wave functions as plane waves in Bloch's notation [46]. Their results show that the tunneling current is proportional to the surface local density of states at the Fermi level and given by

$$I = \frac{32\pi^3 e^2}{\hbar} \frac{\phi^2 R^2 V}{\kappa^4} e^{2\kappa R} \rho_\mu(E_F) \sum_\nu \left|\psi_\nu(\vec{r}_0)\right|^2 \delta(E_\nu - E_F), \tag{2.13}$$

where ϕ is average barrier height, R is diameter of tip curvature, V is the applied bias, and κ is the inverse decay rate for the wave functions into the vacuum given by $\sqrt{2m\phi}/\hbar$. The term in the summation on the right hand side of Equation (2.13) is the density of surface states around the Fermi level (E_F) calculated at the center of the tip apex $\vec{r}_0$. The probability density of the surface wave functions at $\vec{r}_0$ can be approximated as [47]

$$\left|\psi_\nu(\vec{r}_0)\right|^2 \propto e^{-2\kappa(R+d)}, \tag{2.14}$$

where d is the distance between the tip and the sample.

Equations (2.13) and (2.14) are sufficient to give an idea about the meaning of STM images and can show how atomic resolution may look like with a spherical tip. More advanced methods, which also take into account the exact shape of a tip exist [48] but are not discussed here. What is important to notice is that the tunneling current is inversely proportional to the exponential of the distance between the tip and sample, and that constant current images of the STM map the convolution of the tip and sample density of states.

It is important to remember that the starting point of the tunneling current calculation was based on time-dependent perturbation theory and the result is approximate. There are certain limitations not only for Tersoff and Hamann's approach, but also for Bardeen's way of writing matrix elements for tunneling. Today, more detailed theoretical works exists, which defines the tunneling current in more elaborate ways (see e.g. [49]), which are out of scope here.

2.3.2 Scanning Tunneling Microscopy Instrumentation

There are two key developments for an STM instrument, namely, effective vibrational damping and nano-positioning devices. The importance of vibrational stability is clear by considering the fact that typical atomic distances for any type of bulk or surface structure are in the orders of few Ångströms. Therefore to acquire images with atomic resolution a vibrational damping is necessary which reduces movements of tip and sample below the Ångström scale. The STM instrument used to perform measurements reported in this thesis, an Omicron Room Temperature UHV STM 1 [50], has a two-

level vibrational dumping system. First, the laboratory is in the basement to reduce the effects of vibrations in the building (which has no windows and therefore fully isolates the operator from the "beautiful" Swedish weather, too) and the frame on which the UHV chambers are attached is isolated from the floor by placing a semi-elastic material underneath. Second, the whole STM stage (scanner, tip, and the sample) is suspended on springs and further stabilized by an eddy-current damper. Nano-positioning devices are vital to be able to scan the tip over distance on the nanometer scale and to position the tip with sub-Ångström precision (lateral resolution ~ 0.1 Å). For positioning piezoelectric materials are used, which expand or contract depending on the applied electric field. The piezocrystals used in the Omicron STM change their size by approximately 5 nm per volt.

As already mentioned above, there are two different imaging modes of STM, the constant current imaging (CCI) and the constant height imaging (CHI) modes. In the CCI mode, for a certain bias voltage applied, the measured tunneling current is kept constant by adjusting the surface-tip distance with the help of a feedback loop. As the tip is scanned over the surface the voltage applied to the piezomaterial, which is responsible for the movement of the tip in the direction of the surface normal – the z-piezo –, provides a measure of the topography of the surface. In the less commonly employed CHI mode, again for a certain bias voltage, the tip movement in z direction is fixed by keeping the voltage on the z-piezo constant. The tunneling current is recorded to give the topography. Since the tip is not moved in the z-direction, the CHI mode is not appropriate for stepped or rough surfaces, since there is always a danger of crashing the tip into the surface. The advantage of the CHI mode is that the feedback loop is disabled, which implies that neither resolution nor scanning speed are limited by the feedback loop response time.

Figure 2.4 shows a schematic drawing of the Omicron STM setup. A tip carrier plate is attached to three piezoelements x, y, and z. This configuration allows one to exchange tips in situ. The sample is placed in a sample holder (not shown in Figure 2.4) for coarse movement in the x- and z-directions (40 to 400 nm per step), which also allows for in situ sample exchange. Samples are mounted on metallic plates which have high melting temperature and low degassing rates. Tantalum and molybdenum are quite suitable for this purpose and often used as sample plate material.

In CCI mode the tip is scanned in the x-y plane with a saw tooth and step-like voltages applied to the x and y-piezo elements, respectively, with periods of rastering time (t_R). Rastering time is the time which is spent for the tip to come to the same point after completing two line scans (forward and backward) in x direction with a constant y value. During the scan the voltage on the z-piezo is adjusted with the help of a feedback loop so that the current is always equal to the set point value. The value of the bias voltage and the set point current is determined by the operator. The voltage applied to the z-piezo (V_z) with respect to the x- and y-coordinates is stored in the computer, and these values provide a 3D image of the surface.

There exist a couple of different ways to obtain tips for STM measurements. One possibility is to purchase commercial tips from several companies. However, there is a simple and well established way of producing tips in an ordinary laboratory. In the present work home-made tips were used made of tungsten wires chemically etched in a KOH solution. In many cases the tips are introduced into the UHV chamber without any further treatment. Sometimes scanning on metal surfaces or Argon sputtering treatment is used to get atomically sharp and oxide-free tips.

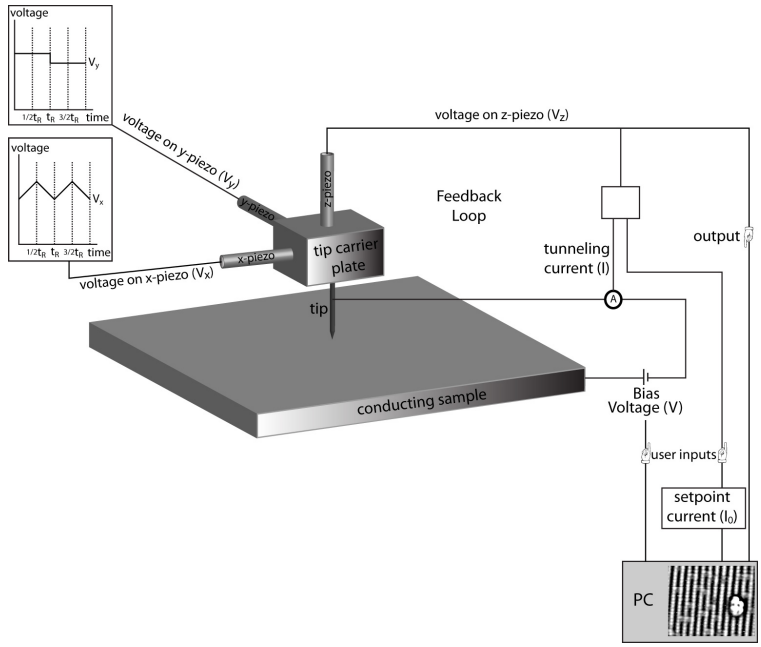

Figure 2.4 A schematic drawing of the Omicron STM setup. The tip is scanned over the surface with x- and y-piezoelements while the current is kept constant (CCI mode) by a feedback loop which adjusts the movement of the z-piezo. The voltages applied to x- and y- piezoelements are respectively saw tooth and step-like in shape with period of the rastering time (t_R).

2.4 Density Functional Theory

The calculation of physical properties of a system, such as a solid material which consists of electrons and nuclei, requires the solution of the Schrödinger equation. It is a second order differential equation which for a given Hamiltonian allows one to in principle calculate the wave function of the system and therefore any other properties. The problem is that, except in a very few cases, it is not possible to solve the Schrödinger equation exactly. Therefore from the very beginning of quantum mechanics some approximation methods have been developed. These methods can be grouped as wave function- and density functional-based theories [51].

In both types of theory the starting point is to assume that the nuclear and electronic degrees of freedom can be decoupled so that the electronic problem can be solved for a set of nuclei fixed in space. In this way the kinetic energies of the nuclei become zero and the contribution of the nucleus-nucleus interactions to the total energy become a constant. This is a reasonable assumption – the basis of the Born-Oppenheimer approximation – since the nuclear motion is very slow compared to the electronic motion because of the big difference in electronic and nuclear masses.

The conventional approach in wave function-based theories is the Hartree-Fock method which approximates the many-body wave function as an antisymmetrized sum of products of single particle

wave functions (the so-called Slater determinant). By applying the variational principle[10] eigenvalue equations (Hartree-Fock equations) are obtained for each of the one-electron wave functions, and this set of equations is solved self-consistently. The major shortcoming of all wave function-based theories is that for an N particle system there are 3N spatial and N spin dimensions. This makes any system with a moderate or even large size an intractable problem.

On the other hand, in density functional theory (DFT) the 4N dimensional wave function is replaced by the electron density which is in any case just a 3-dimensional quantity. Hohenberg and Kohn proved that the ground state-electron density uniquely determines the Hamiltonian and therefore all other properties of the system, and through application of the above-mentioned variational principle they showed that the ground state energy functional has its minimum value for the correct ground state density [52]. Kohn and Sham [53] introduced the machinery to apply DFT to real total energy calculations.

The substantial difference between the DFT and Hartree-Fock methods is that the Kohn-Sham approach is exact, although in practice approximations always have to be introduced. Walter Kohn received the Nobel Prize in Chemistry in 1998 "for his development of the density functional theory" [54].

2.4.1 Fundamentals of Density Functional Theory

The electronic Hamiltonian of a system of electrons and nuclei can be written, within Born-Oppenheimer approximation, as[11] [55]

$$\hat{H} = -\frac{1}{2}\sum_{i=1}^{N}\nabla_i^2 - \sum_{i=1}^{N}\sum_{A=1}^{M}\frac{Z_A}{r_{iA}} + \sum_{i=1}^{N}\sum_{j>i}^{N}\frac{1}{r_{ij}} = \hat{T} + \hat{V}_{Ne} + \hat{V}_{ee}, \qquad (2.15)$$

where the indices $i, j = 1, 2, 3, ..., N$ and $A = 1, 2, 3, ..., M$ refer to the electrons and nuclei, respectively. Z_A represents the atomic number of the A^{th} nucleus. r_{ij} is the distance between the i^{th} and j^{th} electron, and r_{iA} is the distance between the i^{th} electron and A^{th} nucleus. As shown on the right-hand side of the Equation (2.15), the individual terms in the Hamiltonian represent the kinetic energy of the electrons (T), electron-nucleus attraction (V_{NE}), and electron-electron repulsion (V_{ee}), respectively. Hohenberg and Kohn have proven that the Hamiltonian is uniquely determined by the ground state density (ρ_0), and therefore, the total energy and all individual terms of the Hamiltonian can be written as functionals of the ground state density [56]:

$$E_0[\rho_0] = T[\rho_0] + E_{Ne}[\rho_0] + E_{ee}[\rho_0]. \qquad (2.16)$$

In equation (2.16) the system dependent and universal terms can be distinguished as

[10] The variational principle states that the expectation value of the Hamiltonian in terms of the true wave function always is smaller to the expectation value of the Hamiltonian in terms of the approximated wave functions.
[11] In this section atomic units are used.

$$E_0[\rho_0] = \underbrace{T[\rho_0] + E_{ee}[\rho_0]}_{\text{universal}} + \underbrace{\int \rho_0(\vec{r}) V_{Ne} d\vec{r}}_{\text{system dependent}}. \tag{2.17}$$

Unfortunately the exact forms of the universal functionals are unknown.

Kohn and Sham developed the idea of taking the components, which can be calculated exactly, out from universal terms and collect the unknown parts in a term (a "junkyard" [56]) called the exchange-correlation functional. In the kinetic energy functional, the kinetic energy of the non-interacting system ($T_S[\rho]$) and in the electron-electron interaction energy functional the classical Coulomb interaction ($J[\rho]$) terms can be calculated exactly. Both of the "residuals" are collected in the exchange-correlation functional, which includes all many-body effects. Hence, the total energy can be written as

$$E[\rho] = T_S[\rho] + J[\rho] + E_{Ne}[\rho] + E_{XC}[\rho], \tag{2.18}$$

or explicitly

$$E\left[\rho(\vec{r})\right] = -\frac{1}{2}\sum_i^N \langle \varphi_i | \nabla_i^2 | \varphi_i \rangle - \sum_i^N \sum_j^N \iint |\varphi_i(\vec{r}_1)|^2 \frac{1}{r_{12}} |\varphi_j(\vec{r}_2)|^2 d\vec{r}_1 d\vec{r}_2 + \sum_i^N \int \sum_A^M \frac{Z_A}{r_{1A}} |\varphi_i(\vec{r}_1)|^2 d\vec{r}_1 + E_{XC}[\rho(\vec{r})], \tag{2.19}$$

where the φ_i are Kohn-Sham orbitals, which are the solutions to the Kohn-Sham equations

$$\left(-\frac{1}{2}\nabla^2 + \int \frac{\rho(\vec{r}_2)}{r_{12}} d\vec{r}_2 + V_{XC}(\vec{r}_1) - \sum_A^M \frac{Z_A}{r_{1A}}\right)\varphi_i = \varepsilon_i \varphi_i. \tag{2.20}$$

This set of equations is solved self-consistently to yield minimum ε_i, the Kohn-Sham eigenenergies. It is important to keep in mind that the ε_i do not correspond to any physical quantity, except for the ε_i of the highest occupied state [57]. Once the φ_i have been calculated they can be plugged into Equation (2.19) to calculate the total energy of the ground state.

The formalism of DFT which is given in Equations (2.19) and (2.20) is exact; however, in order to solve the Kohn-Sham equations the V_{XC} term, the analytical form of which is unknown, needs to be approximated. The first approximation to the exchange correlation functional is made in the Local Density Approximation (LDA), in which the V_{XC} term is set equal to the value of a homogeneous electron gas with the same electron density at each points of the investigated system. Although such an approximation looks very crude, it has provided quite reasonable predictions and understanding especially for metallic systems [58]. One step forward from the LDA is to include in the calculation of the V_{XC} term not only the electron density of the homogeneous electron gas itself, but also its gradient. This method is called the generalized gradient approximation (GGA), of which there exist different versions widely used in surface science studies, namely, PW91, PBE, RPBE[12].

[12] There are as many acronyms as various exchange correlation functionals in DFT. It is not the purpose of this text to name them all.

Nearly all physical properties of a material somehow can be deduced from calculations of the total energy or total energy differences [59]. (2.19) and (2.20) are the two equations which show how the total energy of a system can be calculated with DFT. However, these two equations are derived for fixed nuclear positions. In order to calculate the most stable structure of a system, the total energy should also be minimized with respect to the nuclear coordinates. This can be achieved by calculating the forces acting on each nucleus and searching through the nuclear coordinate space for the points, at which the forces assume their minimum values. Since changes in nuclear positions affect the electronic Hamiltonian, for each point in nuclear coordinate space, Kohn-Sham equations should be re-solved self-consistently.

2.4.2 Plane Wave Pseudopotential Approach

Many different practical approaches have been developed for solving the Kohn-Sham Equations. The first question to ask is how to form Kohn-Sham orbitals. A possible answer, which fits very well to periodic structures (such as crystals) and which therefore is widely employed in the solid state community, is to use plane waves as a basis set. The Bloch theorem states that, in general, the wave function of an electron in a periodic potential can be written as a product of a function which has the same periodicity as the potential and an arbitrary phase factor. The idea is to expand the periodic function as a series of plane waves to represent the wave functions as [59]

$$\psi_i\left(\vec{r}\right) = \sum_{\vec{G}} c_{i,\vec{k}+\vec{G}} e^{i\left(\vec{k}+\vec{G}\right)\cdot\vec{r}}, \tag{2.21}$$

where $c_{i,\vec{k}+\vec{G}}$ are the expansion coefficients, $\vec{G}$ is a reciprocal lattice vector, and $\vec{k}$ is a reciprocal space vector in the first Brillouin zone. A periodic system should in principle be infinite, which means that the expansion in Equation (2.21) should contain an infinite number of plane waves, which should be calculated in an infinite number of k-points. There are two important observations, which turn this infinite expansion into a computationally tractable problem. Firstly, the wave functions are similar in k-points which are close to each other; therefore, it is possible to reduce small regions in k space to single k-points. Secondly, the expansion coefficients for low kinetic energies are more important than those for high kinetic energies, which allow an energy value (cutoff energy) to be set, where higher-energy terms can be ignored [59]. Unfortunately, there is no simple way of knowing what the suitable k-point grid or energy cutoff value are, and for each system the convergence of the physical properties of interest with respect to these two parameters needs to be checked.

One serious problem with the plane wave basis set is that in the core energy regions, where a strong attractive potential exists, the wave functions tend to oscillate very strongly. A suitable representation of these oscillating wave functions requires a large number of plane waves. This problem is typically circumvented by replacing the nuclei together with the core electrons with a pseudopotential, which reproduces certain properties of the core region, but makes the potential and oscillations in the wave functions less drastic or *softer*. Such a replacement can be justified by the fact that the chemistry of a compound or solid is actually determined by the valence electrons, while the core levels are not involved in the determination of the chemical properties. The introduction of pseudopotentials has one more advantage for the reduction of the computational load, namely, since the core electrons are excluded from the calculation, the number of electrons in the system is reduced.

For reliable calculations pseudopotentials need to have certain properties: (i) the energy eigenvalues of the valence electrons should have the same values as for full atomic calculations, (ii) the wave function and its first derivative should be continuous at the boundary of the core region, and (iii) the integrated charge density in the core region should be the same for the atom with pseudopotential and the complete atoms. The latter is called norm-conservation [60]. There exists a certain type of pseudopotentials, which were developed by Vanderbilt [61] and calculated by relaxing the norm-conservation condition. These pseudopotentials are called *ultrasoft* pseudopotentials and significantly reduce the number of plane waves in the wave function expansion for a given accuracy.

It is not very uncommon that the structures which are desired to be calculated are non-periodic, such as a molecule in the gas phase, surface of a certain material or combination of both, i.e. a surface adsorbate. The proper application of the plane wave approach to these cases requires the repetition of non-periodic structures in space. For this purpose so-called supercells are employed. A supercell is a volume in real space which is repeated in all three dimensions and contains the non-periodic structure to be calculated. This method creates an artificial structure which should be treated with caution. In the calculation of molecular adsorption on a surface it is important to make sure (i) that there is a vacuum region in the direction of the surface normal which is "thick" enough to avoid artificial interactions between the slabs, (ii) to include enough layers of atoms to ensure that the surface structure is modeled properly, and (iii) to keep in mind that the calculations are performed for certain coverages different than zero induced by the limited lateral size of the supercell. For calculations of different structures the convergence of properties of interest with respect to these parameters should also be checked as in the case of the k-point grid and cutoff energy.

In the present work the Cambridge sequential total energy package (CASTEP) [60] has been used to perform DFT calculations. The program is based on the plane-wave pseudopotential approach and able to perform various calculations with many different exchange-correlation functionals. The code was initiated by Mike Payne from Cambridge University in 1986 [60] and further developed and maintained by the Castep Developers Group [62].

Chapter 3

Materials

In this chapter the structure and properties of two oxide surfaces, namely of rutile TiO_2(110) and a ultrathin FeO(111) grown on a Pt(111) surface, and four different molecules, *L*-cysteine, *L*-cystine, S-methyl-*L*-cysteine, and the Zinc-protoporphyrin IX, are described. The intention is to present the most relevant properties of these materials and to motivate why the surface science community studies them. This will be exemplified through relevant literature. The last section of the chapter is devoted to the description of gold clusters and past and current efforts for understanding how their catalytic activity is linked to their atomic and electronic structure.

3.1 The Rutile TiO_2(110) Surface

Titanium dioxide is a semiconducting material with a band gap of around 3 eV. There are three main natural polymorphs of TiO_2, rutile, anatase, and brookite. Surface science investigations focus mainly on the surfaces of rutile and anatase. TiO_2 has wide scientific and industrial applications and is one of the most widely used model systems for metal oxide studies [63]. Rutile TiO_2, and especially its (110) surface, which is more stable than the other low index surfaces [64], have been investigated thoroughly by both experimental and theoretical techniques. The interest in this surface for the work of this thesis is threefold: it is a suitable model system for the study of organic-inorganic interfaces (cf. subsection 1.2.1), for heterogeneous catalysis of CO oxidation (cf. subsection 1.2.2), and for dye-sensitized solar cells (cf. subsection 1.2.3).

The rutile TiO_2(110) surface consists of six- and five-fold coordinated Ti atoms and three- and two-fold coordinated (bridging) O atoms. The excess charge resulting from dangling bonds is compensated by opposite charges on the Ti and O atoms, which results in a neutral surface with no dipole moment in the [110] direction [63]. Both bulk and surface defects have substantial influence on the electronic structure and chemical properties of the material. The bulk defects reduce the TiO_2 crystal (n-type doping) and make it a fairly good conductor, which can be used in both STM and XPS investigations. The most important surface defects are bridging oxygen vacancies and, as discussed recently, titanium interstitials, both of which are active surface sites for the adsorption and decomposition of various species.

Panels (a) to (c) of Figure 3.1 show the most commonly analyzed deep/shallow core and valence levels of the rutile TiO_2(110) surface. In photoemission studies the defect states, which are observed in the band gap at ~0.8 eV binding energy, are generally attributed to reduced positive charge on Ti atoms [65]. However there is a current debate about the origin of these defect states either resulting from oxygen vacancies on bridging oxygen rows [66-68] or sub-surface Ti interstitials [69-71]. DFT

calculations show that, in order to obtain correct values for the physical properties of the surface, such as surface energy and work function, a relatively high number of TiO_2 layers should be used to model the surface [72]. Further, defects are problematic in theoretical calculations. Introduction of bridging oxygen vacancies are both found to [73] and not to [74] reproduce the defect states in the gap. At the same time, Ti interstitials have been found to produce the band gap state [69]. In Figure 3.1 (d) the structure of the rutile TiO_2(110) surface is shown with the conventional unit cell indicated by the dashed rectangle. In Figure 3.1 (e) a six-layer non-optimized bulk-terminated slab of TiO_2 is shown; the optimized geometry is presented in Figure 3.1 (f). Here the atoms of the two bottom layers were fixed in their bulk positions. Both the five-fold coordinated Ti atoms and two-fold coordinated O atoms of the surface are pulled towards the bulk as a result of relaxation. In Figure 3.1 (g) to (j) STM images with different sizes of the rutile TiO_2(110) surface are shown. The outlined square area in panel (g) [(h)] is shown in panel (h) [(i)]. In panel (j) a ~10×10 nm^2 image with atomic resolution is presented. In STM images of the TiO_2(110) surface bright and dark rows are attributed to Ti and O rows, respectively [75]. The bright spots on dark rows can be attributed to either bridging oxygen vacancies or H atoms adsorbed on bridging oxygen rows [76].

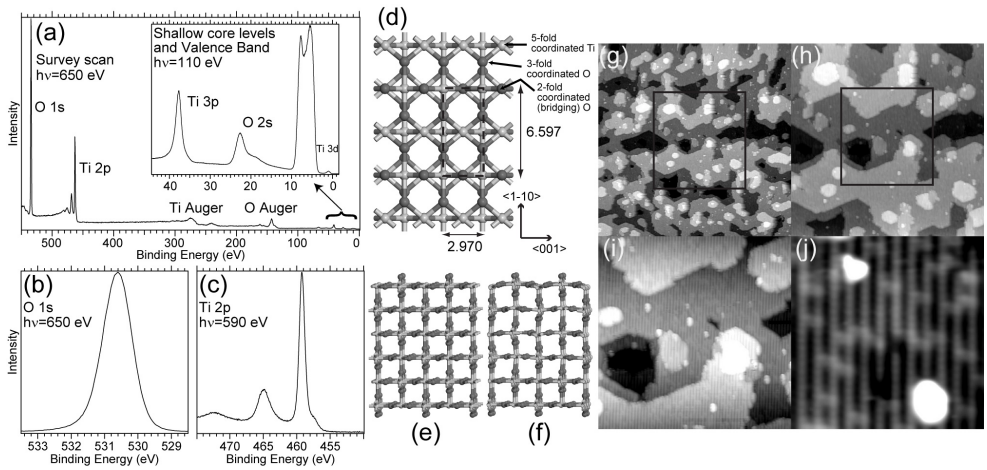

Figure 3.1 Some experimental and theoretical aspects of the rutile TiO_2(110) surface. In **(a)-(c)** most commonly analyzed deep/shallow core and valence levels are shown. Photon energies are given for each spectrum. In **(d)** the structure of the surface as viewed from the [110] direction is shown. The dashed rectangle is the conventional unit cell of the surface with the dimensions given in Å. In **(e)** a bulk-terminated 6-layer slab and in **(f)** the result of geometry optimization are shown. The two bottom layers were fixed to their bulk positions during optimization. In **(g)** a ~200×200 nm^2, **(h)** ~100×100 nm^2, **(i)** ~50×50 nm^2, and **(j)** ~10×10 nm^2 STM images are shown. The rectangle in **(g)** [**(h)**] is re-scanned in **(h)** [**(i)**].

The adsorption of a variety of molecules on the rutile TiO_2(110) surface has been studied with many different motivations, and a very nice survey can be found in the review article by Ulrike Diebold [63]. The carboxylic acids, which are molecules that contain a carboxylic group (–COOH), are closely related to the work presented here. The adsorption of formic acid (H–COOH) [77-80], acetic acid (CH_3–COOH) [81], oxalic acid (HOOC–COOH) [82] and more complex carboxylic acids [83-85] on TiO_2(110) have been investigated. It is found that all these molecules loose a proton from their carboxylic groups upon adsorption and bind to the five-fold coordinated surface Ti atoms as

carboxylates. In terms of UHV adsorption of amino acids on rutile TiO_2(110) surface, literature is not very extensive: glycine [86-88], phenylalanine [89], and proline [90] are the only three amino acid molecules which have been studied previously. For these amino acids a similar adsorption behavior to that of other carboxylic acids has been observed.

3.2 Ultrathin FeO(111) on Pt(111) Surface

The ultrathin FeO(111) grown on a Pt(111) surface was first observed by low energy electron diffraction and a structural model was proposed in the late 1980s [91]. This model was slightly revised in the early 1990s [92] to give the currently accepted form. The ultrathin FeO(111) is produced by deposition of Fe on a Pt(111) substrate at room temperature, followed by an oxidization step at 500 °C for 2 minutes in a ~10^{-6} mbar O_2 atmosphere. This preparation method results in the growth of FeO bilayers on the Pt(111) substrate in a layer-by-layer mode up to 2-3 bilayers. At later stages of growth an iron oxide with a different stoichiometry is observed [93]. The lattice constant of a complete bilayer of FeO(111) (3.09Å) is ~10% larger than the lattice constant of the supporting Pt(111) surface, and therefore a moiré pattern is observed. In addition, the FeO lattice is rotated by ~0.6° relative to the support lattice. Two different orientations of the O layer on top of the Fe layer result in two different structures of the moiré pattern; however, only one structure is commonly observed in STM, the schematic drawing of which is shown in Figure 3.2 (a). In the moiré structure, which has a periodicity of ~26 Å, three different high symmetry domains are formed, which are indicated by triangles and letters, namely, T for top, F for fcc, and H for hcp domains in Figure 3.2 (a). These different high symmetry domains can be used as a template for cluster and molecule growth, since molecules/atoms often prefer to adsorb in one of the domains [94]. In a combined X-ray photoelectron diffraction, LEED, and STM study Kim et al. [95] have shown that the oxygen atoms are located 0.65 Å above the Fe atoms. A side view of the model along the dashed line in Figure 3.2 (a) is shown in Figure 3.2 (b). For the clean FeO(111) the assignment of Fe and O atoms from the STM pictures is not a straightforward task. Their identification has been made possible by adsorption of gas species in their preferred adsorption sites [96,97]. In Figure 3.2 (c) a ~10×10 nm^2 STM image of the FeO(111) is shown with atomic resolution. A moiré pattern is observed clearly.

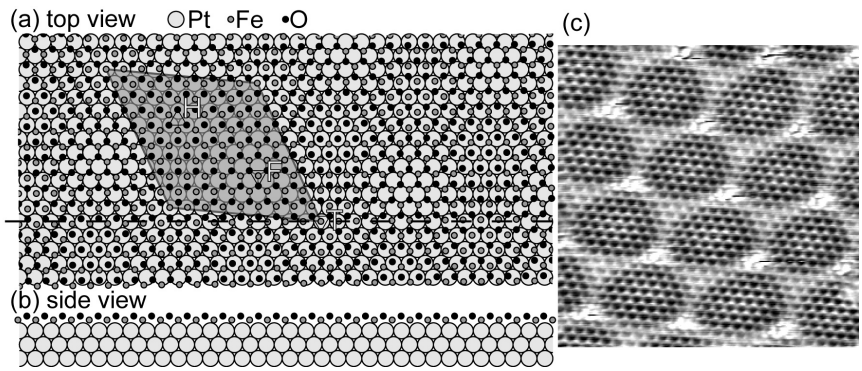

Figure 3.2 (a) Model of observed structure of FeO(111) thin film on Pt(111) surface as viewed from on top and **(b)** from the side. Unit cell of moiré pattern is shown as a shaded parallelogram in **(a)** together with high symmetry domains, T for top, F for fcc, and H for hcp domains. In **(c)** a ~10×10 nm^2 STM image is shown.

3.3 Molecules

Two different classes of organic molecules have been the subject of this thesis. *Amino acids*, on the one hand, are the building blocks of proteins and thus essential for life. They possess a high chemical variability due to the possibility of varying the side groups, and the structural properties of the molecules attract interest in different applications of surface science. *Porphyrins*, on the other hand, are macrocyclic molecules which occur with variety of side groups and metal centers. Metal porphyrins, i.e., porphyrins with a metal atom incorporated in the center, are of particular interest in organic solar cell applications.

Twenty different amino acids are the constituents of all proteins in human body. Glycine, the smallest amino acid[13], consists only of an amino ($–NH_2$) and a carboxylic (–COOH) group attached to each other by a $–CH_2–$ bridge. More complex amino acids, three of which are used as adsorbates in this thesis and shown in Figure 3.3 (a)-(c), are formed by attachment of different side groups to this fundamental backbone. There are two important structural properties of amino acids: first, depending on the phase (solid or gas) and pH value of the solution in which amino acids are dissolved, different zwitterionic forms are observed [cf. Figure 3.3 (d)], and second, amino acids are chiral molecules and all natural amino acids are left handed. This property is indicated by a letter *L* (from *laevus* in Latin which means on the left side) in front of the name of the molecule.

L-cysteine is the only natural amino acid which contains a sulfur atom in the form of a thiol (–SH) side group in its structure. The thiol group has an important role for the stability of proteins and their folding through formation of disulfide (–S–S–) bonds. Two *L*-cysteine molecules can, through an oxidation reaction, attach to each other by a disulfide bond to form *L*-cystine. The properties of *L*-cysteine can be adjusted by changing the structure of the side groups; for example, the thiol group can be replaced by a $–S–CH_3$ group, and in this case the molecule is called S-methyl-*L*-cysteine. Although both *L*-cystine and S-methyl-*L*-cysteine are amino acids they are not members of the twenty natural amino acids family.

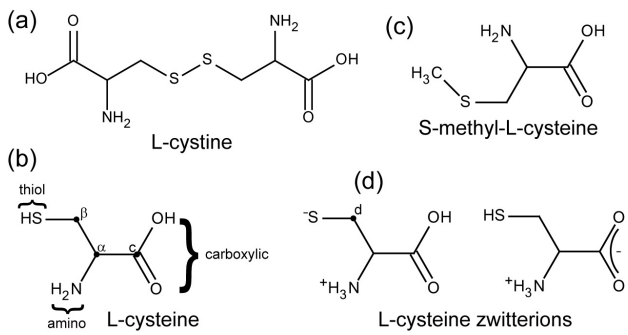

Figure 3.3 Molecular structures of three amino acids: **(a)** *L*-cystine, **(b)** *L*-cysteine, **(c)** S-methyl-*L*-cysteine, and **(d)** two different zwitterions of *L*-cysteine. In **(b)** the different functional groups and carbon atoms of *L*-cysteine are labeled.

There are several aspects which make amino acids interesting molecules from a surface science point-of-view. Firstly, they are suitable molecules for modeling organic-inorganic interactions;

[13] In principle the smallest of all amino acids is carbamic acid (NH_2–COOH) which is not a stable molecule under normal conditions.

secondly, different functional groups makes them good candidates for surface self-assembly studies, and, finally, their chirality are of interest to chiral surface patterning and catalysis. The first two surface science studies which were concerned with adsorption of *L*-cysteine, treated its adsorption from solution onto UHV-prepared Ti films monitored as a function of pH [98] and the other both from solution and through UHV sublimation onto the Cu(111) and Au(111) surfaces [99]. The adsorption of *L*-cysteine on different surfaces of gold [100-103] and copper [104-106] was later revisited and studied in more detail by different groups with different techniques. In addition to these studies, the adsorption of *L*-cysteine on two more metal surfaces has been investigated, namely Pt(111) [107] and Ag(110) [108]. The bonding mechanism of *L*-cysteine to the metal surfaces is found to be different for different substrates. To the gold surface the molecules bind through their deprotonated thiol groups in the zwitterionic phase, while on copper all three functional groups form bonds to the surface, but the strongest bond being formed via the thiol group. There is a certain gap in literature between the wide range of *L*-cysteine adsorption studies compared to adsorption study of *L*-cystine [109] and S-methyl-*L*-cysteine which, to my knowledge, has not been studied at all.

Porphyrins are organic molecules which are constituents of some very important natural complex structures such as hemoglobin and chlorophyll. A porphyrin macrocycle is formed by four pyrrole rings bonded to each other through methine (=CH–) bridges [see Figure 3.4 (a) and (b)]. In a physiological environment usually some metal atoms are coordinated to the center of the molecule. The adsorption-desorption properties of small molecules to these metal centers are quite important in the utilization of these molecules. For example, the Fe-porphyrin in red blood cells is responsible for the oxygen/carbon monoxide transport in the body, where Fe is the ligand on which the transported molecule is adsorbed. Various possible applications of porphyrins, such as catalysis [110], chemical sensing [111], self assembly [112], and information storage [113], are at the focus of the interest of the surface science community. The changes triggered by the adsorption of the molecules on different surfaces, magnetic properties of metallic centers, and the effects of adsorption of small molecules on metallic centers to modify the properties of the porphyrins are the type of questions which are studied in current research.

In Figure 3.4 (c) the molecular structure of the Zinc-protoporphyrin IX is shown, which is a porphyrin molecule with three different side groups and a Zn metal in the center. The zinc-protoporphyrin IX is used as a dye molecule in emerging solar cell applications [17]. The carboxylic groups of propionic acid anchor the molecule to TiO_2 clusters, and the properties of the molecule can be changed by adsorbing smaller ligands.

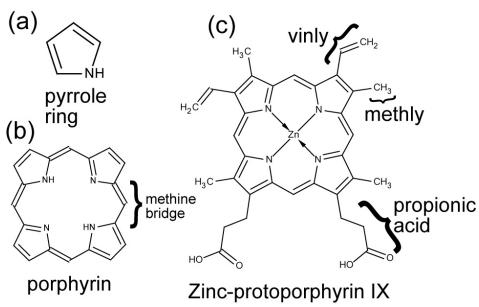

Figure 3.4 Molecular structures of **(a)** a pyrrole ring and **(b)** a porphyrin macrocycle, which consist of four pyrrole rings attached through methine bridges, and **(c)** a Zn-protoporphyrin IX, which is a porphyrin macrocycle with three different side groups and a Zn metal coordinated in the center.

3.4 Gold Clusters

Although gold is known to be the most inert metal [114] and hence considered as catalytically inactive, Haruta and co-workers have shown that Au clusters with a certain size, prepared in a specific way and supported on different oxide substrates have a high catalytic activity for several different reactions [115]. The catalytic mechanism is still not well understood, but different models have been proposed as mentioned in subsection 1.2.2. The efforts to understand the mechanism are focused mainly on the determination of the atomic and electronic structure of Au clusters of different sizes on different support materials and the chemical activities of these clusters towards the activation of CO and O_2.

A particular interest exists for Au/TiO_2, since this system can be used as an active catalyst for the CO oxidation reaction at significantly lower temperatures as compared to conventional catalyst materials [116]. However, beginning from the very early studies [10] it has been well-known and also presented experimentally [13,117] that sintering of the Au clusters is a major problem, which degrades the long term stability as a catalyst, since clusters show high activity only at a certain sizes. Several possible methods for stabilizing the clusters under typical reaction conditions have been reviewed recently [118]. Additional efforts exist for tailoring the size and chemical properties of Au clusters in a controlled way through ligand protection especially with thiol species [119,120].

The Au/TiO_2 system has been investigated thoroughly from many different perspectives and with many different methods. The main focus of surface science studies has been on rutile the $TiO_2(110)$ surface, which is being used as a model substrate. In the most recent theoretical studies [121-123] it has been shown that the charge state of Au_n clusters ($n>10$) and their interaction with the substrate strongly depend on the reduction (through bridging oxygen vacancies) and oxidation (through oxygen adatoms) state of the rutile $TiO_2(110)$ surface. The calculations predict neutral, positively, and negatively charged clusters on stoichiometric, oxidized, and reduced substrates, respectively. It has also been shown that the charge is not homogenously distributed among the atoms of the cluster and adhesion is stronger on non-stoichiometric surfaces. In line with the theoretical calculations a recent high resolution STM study [124] revealed that bridging oxygen vacancies and oxygen adatoms on five-fold coordinated Ti rows are the nucleation sites for Au clusters at early stages. Other STM studies [117,12], in which higher Au coverages were investigated, report an almost homogeneous distribution of clusters on the reduced and oxidized surfaces in the ~0.2-0.7 ML coverage range.

Au clusters supported by the rutile $TiO_2(110)$ surface have also been studied extensively by photoelectron spectroscopy. The net result of increasing cluster size is a shift of the Au 4f levels to lower binding energies (toward the metallic Au 4f energy) accompanied by a decrease in the width of the peaks. However there is no solid agreement in literature as to what is the cause of these changes and it is debated whether the shift arises due to initial or final state effects. Zhang et al. [125] related the change of the Au 4f peak binding energy to the coordination of Au atoms in the clusters and electronic screening effects. In the study changes in binding energy of the substrate core levels were observed and interpreted in terms of band bending. Howard et al. [126] assigned the binding energy shifts and changes in width of the Au 4f peak to the positive charge left on the clusters in the photoemission process. However, it was pointed out that the same reasoning could not explain the

behavior of the photoemission onset, where initial state effects also play a role. In a combined UPS and STM study Minato et al. [127] concluded that the evolution of the valence band photoemission can be explained by negative charge transfer from surface defects to the Au clusters. In a comparative study of Au cluster growth on NiO(001) and TiO_2(110) Okazawa et al. [128] concluded from the observation of a work function reduction and binding energy shift that there is negative charge transfer from the Au clusters to the TiO_2(110) substrate for a certain coverage range (0.15-1.5 ML). Later the same group studied the growth of Au on reduced and stoichiometric TiO_2(110) in more detail [129] and reached similar conclusions. Jiang et al. [130] studied adsorption of Au on the reduced and stoichiometric TiO_2(110) surfaces and reported different results for the reduced surfaces in comparison to previous studies. These authors observed a shift in the Au 4f line, initially towards lower binding energies at low coverage, and, after certain threshold coverage towards higher binding energies. The conclusion was that on the reduced surfaces – but, in contrast, not on the stoichiometric surface – negative charge transfer takes place from the surface defects to the Au clusters. Additionally, in an Auger parameter analysis study of Ni clusters on rutile TiO_2(110) [131] it was concluded that for decreasing cluster size initial and final state effects cause shifts to lower and higher binding energies, respectively. Initial state effects were assigned to both the negative charge transfer from the clusters to the substrate and a relative decrease of surface component of the clusters. Later the same group reported that on reduced surfaces negative charge transfer occurs from the substrate to the clusters instead [132]. However, it should be noted that Bagus et al. [133] expressed doubts about the validity of the Auger parameter analysis studies in which the shallow valence states involved in the Auger process.

Current literature concerned with the growth of Au clusters on the reduced rutile TiO_2(110) surface can be summarized in the following way: According to STM results Au atoms start to nucleate at the defects of the surface (bridging oxygen vacancies and step edges). DFT calculations show that these clusters acquire negative charge from the substrate and that the charge is localized at the cluster-surface interface. However, the observed shift of the Au 4f level to lower binding energy with increasing cluster size cannot only be interpreted in terms of this and other initial state effect. The negative charge density on the Au clusters decreases with increasing cluster size since the number of available surface defects (the source of the negative charge) is limited, and such a decrease should result in a relative shift not to lower, but higher binding energy with increasing cluster size. This makes clear that final state effects have a significant and opposite effect on the binding energy changes. As already pointed out in various photoemission studies an increase in cluster size leads to a better screening of the core hole created in the photoemission process, which results in a shift toward lower binding energy. The decrease in FWHM of the Au 4f line with increasing cluster size is generally interpreted as a final state effect.

Chapter 4

Results

In this chapter I summarize the results of the **Papers** on which the work of this thesis is based and highlight the most interesting points. Instead of reprinting measured spectra, images, or calculated structures I refer to the figures in the **Papers**. I do not re-cite any literature in this chapter and instead the reader is referred to the corresponding sections of the thesis.

4.1 Adsorption of Amino Acids on the Rutile TiO_2(110) Surface

The adsorption of three amino acids, *L*-cysteine, *L*-cystine, and S-methyl-*L*-cysteine on the rutile TiO_2(110) surface are investigated. The carboxylic groups of all three molecules are found to be deprotonated, which indicate that, if sterically possible, bidentate bonds between the equivalent O atoms of the deprotonated carboxylic groups and the surface Ti atoms are formed [Figure 2 (a) in **Paper 1** and Figure 2 in **Paper 4**]. This is not a surprising observation and just validates numerous studies in literature (see section 3.1), which have shown that carboxylic acids (R–COOH) adsorb on the rutile TiO_2(110) surface as carboxylates ($R–COO^-$). What is interesting is the observation of different dissociation pathways for *L*-cysteine and *L*-cystine molecules on the surface. It is found that the thiol (–SH) groups of *L*-cysteine are deprotonated and bind to the available surface bridging oxygen vacancies [Figures 4 and 5 in **Paper 1**]. The disulfide (S–S) bonds of a fraction of the *L*-cystine molecules break and the fragments bind to both the bridging oxygen atoms and vacancies of the surface through their active sulfur ends. In contrast, the methylmercapto ($–S–CH_3$) side group of the S-methyl-*L*-cysteine is found intact [Figure 3 in **Paper 4**]. In case of adsorption of *L*-cysteine and S-methyl-*L*-cysteine the amino groups of the molecules are found to be in their neutral form ($–NH_2$) at low coverages and the protonated form ($–NH_3^+$) for higher coverages [Figure 3 (a) in **Paper 1** and right panel of Figure 4 in **Paper 4**]. This is in agreement with literature (see section 3.3). However, for *L*-cystine adsorbates in addition to the neutral amino groups at low coverages free amino groups, i.e., amino groups which are not involved in any hydrogen bonding, are observed for higher coverages [left panel of Figure 4 in **Paper 4**]. To the best of my knowledge this observation is the first in literature. The formation of free amino groups is a size-related effect. As the adsorption sites of the surface are filled for increasing coverages the molecules are forced into a more upright geometry. Another interesting observation for *L*-cystine is that, independent of coverage, some of the deprotonated carboxylic groups are found not to attach to the surface [right panel of Figure 5 in **Paper 4**]. In Figure 4.1 different species which are observed for adsorption of *L*-cysteine, *L*-cystine, and S-methyl-*L*-cysteine on the rutile TiO_2(110) surface are shown schematically. Experimental S $2p_{3/2}$, N 1s, and C 1s binding energies of some atoms are indicated. In **Paper 3** DFT is employed to calculate the relative stabilities of different adsorption geometries of *L*-cysteine on the rutile TiO_2(110) surface. In line with the experimental results it is found that the adsorption geometries

with deprotonated thiol groups, which co-bond to bridging oxygen vacancies, are more stable than the adsorption geometries on the stoichiometric surface.

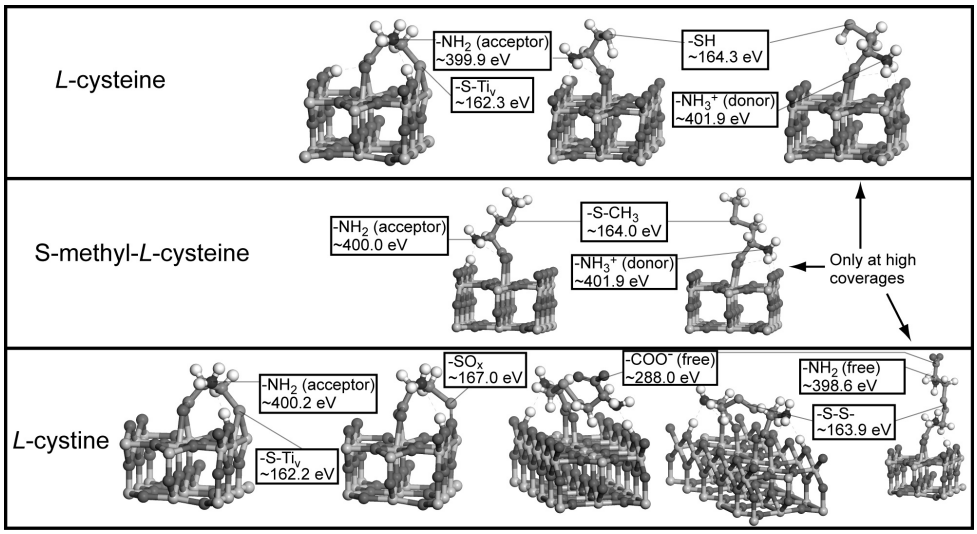

Figure 4.1 Schematic presentation of different adsorption geometries of *L*-cysteine, S-methyl-*L*-cysteine, and *L*-cystine on the rutile TiO_2(110) surface. For some atoms XPS binding energies are provided. Dark and light gray atoms of the surface are O and Ti, respectively. In the molecules the darkest colored and white are N and H atoms, respectively. The gray tone of C and S atoms are almost the same, however, since the binding energies of the S atoms are given they can be distinguished from the C atoms.

4.2 Co-adsorption of Gold and *L*-cysteine on the Rutile TiO_2(110) Surface

In **Paper 2** the co-adsorption of gold cluster and *L*-cysteine on the rutile TiO_2(110) surface is studied by XPS. The main intention of the paper is to investigate both the effect of pre-adsorption of a thiol-containing molecule on cluster size and deposition order on cluster-molecule, cluster-surface, and surface-molecule interactions. The study is based on the following empirical knowledge: (i) at room temperature gold deposition leads to the formation of gold clusters on the rutile TiO_2(110) surface and the size of the gold clusters is proportional to the amount of gold deposited, and (ii) the positive charge left on the clusters in the photoemission process is responsible for the changes in Au 4f binding energy and full width at half maximum (see section 3.4). It is shown that for the same amount of gold deposited almost a factor of three smaller clusters are formed if the surface is pre-covered by half a monolayer of *L*-cysteine. The main interaction between the gold and molecules is through the molecules' deprotonated thiol groups. If gold is deposited on top of an *L*-cysteine layer the clusters aggregate on the molecular layer which leads to deprotonation of the non-bonded thiol groups. Deposition of gold beyond approximately four gold atoms per thiol group results in the release of all deprotonated thiol groups from the surface defects [Figure 2 (a) in **Paper 2**]. When gold is deposited first, the clusters are larger and a smaller fraction of the post-deposited *L*-cysteine molecules interact with the gold clusters. To a large extent, this is a result of the three dimensional

grow of the gold clusters. For bigger clusters more of the gold atoms are in the "bulk" of the cluster and therefore not available for coordination to the thiol groups. Interestingly, almost a constant fraction of the molecules interact with the surface defects irrespective of gold coverage [Figure 2 (b) in **Paper 2**]. In Figure 4.2 the results of **Paper 2** are shown schematically. For the different sulfur species the experimental S $2p_{3/2}$ binding energies and calculated radii of gold clusters are given.

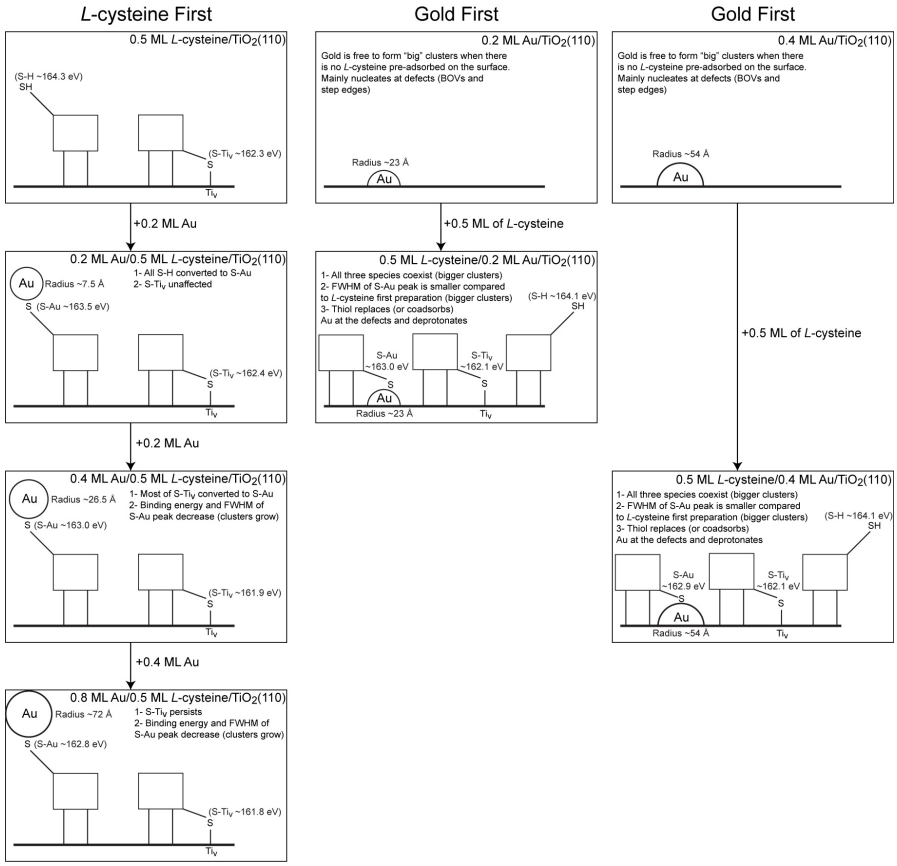

Figure 4.2. Schematic representation of the model developed for the co-adsorption mechanism of gold clusters and *L*-cysteine. The radii of the gold clusters and S $2p_{3/2}$ binding energies are given. Although studied in **Paper 2**, the 0.8 ML gold coverage is not shown.

4.3 Zwitterionic *L*-cysteine

It is well-known that amino acid molecules are in a zwitterionic state in aqueous solution. Tabulated acidity constants (pK_a) of the different functional groups of *L*-cysteine molecule manifest that the carboxylic group is the one which should deprotonate first to form $–COO^-$ and H^+ in solution. The basic amino group receives the H^+ and turns into $–NH_3^+$. In **Paper 5** it is shown that for a thick film

(<40 Å) of *L*-cysteine grown at 100 K it is mostly the thiol groups of the molecules provide protons to the amino groups, and only a small fraction of the carboxylic groups are deprotonated.

4.4 Zinc-protoporphyrin IX on the Rutile TiO_2(110)

In **Paper 6** the adsorption of Zinc-protoporphyrin IX is studied by XPS and NEXAFS spectroscopy. It is found that the molecules anchor to the surface through their deprotonated carboxylic groups, and hydroxyl oxygen atoms of the carboxylic acid are observed only for multilayer preparations [Figure 2 in **Paper 6**]. Mostly at submonolayer and partially at monolayer coverages the molecules are found to be tilted toward the surface, which indicates an additional interaction between the surface and the other groups of the molecule. However, as the coverage increases the molecules adopt a more upright adsorption geometry [Figure 4 in **Paper 6**]. At monolayer coverage the zinc atom is found to be pulled out from the center of the molecule [Figure 5 in **Paper 6**].

4.5 Gold Clusters on Partly Reduced FeO(111)/Pt(111)

In **Paper 7** it is shown from a combined XPS and STM investigation that the oxygen vacancies on an ultrathin FeO(111) act as nucleation sites for gold clusters. Adsorption of atomic hydrogen succeeded by a thermal treatment results in desorption of water and hence in a partly reduced surface. In this way triangular oxygen dislocation loops are formed [Figure 3 (a) in **Paper 7**]. When gold is deposited on the reduced surface the oxygen vacancies are fully replaced by gold clusters [Figure 3 (b) in **Paper 7**]. Moreover, clusters which are formed on the reduced surface are more active towards CO adsorption [Figure 2 in **Paper 7**] than clusters formed on the stoichiometric surface. This is interpreted as a formation of smaller clusters on a surface with defects.

Chapter 5

Concluding Remarks and Future Projections

I believe that the results presented in this thesis will contribute to current research efforts in relevant fields, mostly on the fundamental and partly on the applied level. After almost five years of work my colleagues and I were able to show how three different sulfur-containing amino acids interact with a metal oxide surface. We demonstrated experimentally that the different functional groups of the molecules as well as the defects on the surface play important roles in stabilizing the adsorbates. The experimental results, which indicate the importance of surface defects, were also supported by theoretical calculations. At least in principle, we also showed that a thiol-containing molecule or a well-organized defect structure on an oxide surface can be used as a "template" for growing gold clusters with certain sizes. In the case of the ultrathin iron oxide film it was even demonstrated that these gold clusters are active for CO bonding. As a surprising result out of the main research line we showed that at a certain temperature there is an unexpected competition between proton transfer from the thiol and carboxylic group to the amino group, and in contrast to textbook expectations in thick cysteine films formed at low temperature the thiol groups act as hydrogen donors rather than the carboxylic groups. Finally, we found that a metal porphyrin molecule may interact so strongly with the oxide surface that the central metal atom is detached from the molecule. This may lead to the loss of functionality of this molecule.

During time of my PhD education I not only carried out the research activities, the results of which are presented in this thesis, but I also accumulated a certain amount of knowledge and experience in the field. In the following paragraphs I will comment about what can be done to take the results of this thesis further, and what kind of information is lacking or interesting.

Firstly, I find the debate related to the origin of the defect states of the rutile TiO_2(110) surface a highly interesting issue. I believe that photoelectron spectroscopy can provide more valuable information related to assignment of the defects. The measurement of the defect states in the band gap with variable surface sensitivity – by changing the emission angle rather than the photon energy – can provide information about the exact position and hence type of the defects. These measurements can be performed on the surfaces with high defect concentration as well as stoichiometric, oxidized, and hydroxylated surfaces.

Amino acid adsorption studies on the rutile TiO_2(110) surface can be diversified in two directions. First, more of the natural the amino acids can be studied since there are number of them, e.g., tyrosine, serine, methionine, histidine, valine, threonine, and alanine, which have been the subject of UHV adsorption studies on various surfaces but not on the rutile TiO_2(110) surface. Second, adsorption under more "realistic" conditions can be studied such as the adsorption on hydroxylated or oxidized TiO_2(110) surfaces or co-adsorption with water. After assessment of the most stable

adsorption geometries of *L*-cysteine on the surface with DFT, core level shifts calculations may be performed and the reactivity of Ti interstitials toward the adsorption of *L*-cysteine molecules might be studied. Obviously, DFT can be employed to verify the observed species in the case of adsorption of other amino acids. I performed some preliminary STM experiments concerning the adsorption of *L*-cysteine on the rutile TiO_2(110) surface and acquired some interesting results. However, I did not have enough time to put the story into a shape, which could be presented here. Room temperature STM measurements are certainly possible and can provide more insight into the adsorption of amino acids on the rutile TiO_2(110) surface.

The project on the co-adsorption of gold and *L*-cysteine can certainly be continued by additional studies concerning the adsorption of CO and/or O_2 molecules or the effect of increasing temperature on the cluster size. Additionally, different coverages of pre-adsorbed *L*-cysteine might be studied to elucidate the influence of coverage on the cluster size. It is also conceivable to study the co-adsorption of gold with different thiols. Two possible choices would be the thioglycolic (HS-CH_2-COOH) and 3-mercaptopropionic (HS-CH_2-CH_2-COOH) acids. In fact, we performed some preliminary XPS experiments with 3-mercaptopropionic acid on the rutile TiO_2(110) surface. The main issue with these two molecules is that they have low melting temperatures and therefore sublimation of these molecules in UHV conditions are challenging. Another direction to proceed towards are co-adsorption studies using selenium as a substitute for sulfur. In the periodic table selenium is just one row the sulfur and therefore has similar properties. For example, there exists a molecule called selenocysteine, in which the sulfur atom is replaced by selenium.

One question which can be asked about the unconventional zwitterionic phase of *L*-cysteine is: what is the exact temperature at which this unexpected behavior is observed. For this purpose thick films prepared at 100 K can be warmed up in a stepwise manner and XPS measurements can be performed in each step or alternatively thick films can be prepared at different temperatures. Structural effects can also be interesting: some other molecules which contain amino, thiol, and carboxylic groups with different sizes can be tested. Although I do not consider it very likely, the substrate might change the properties of the thick films grown on them. These effects could be checked out. Possibly, the TiO_2 substrate triggers some structural modifications and fingerprints are left all the way up to multilayers.

One direction toward which surface science is heading are high pressure studies using techniques which traditionally only have been performed in UHV. The Au/FeO(111) project can certainly be improved in this respect. Stability (against sintering) of gold clusters grown on partly reduced oxide film can be studied in high pressures of CO and/or O_2. Further, catalytic activity measurements can be performed.

Chapter 6

References

[1] C. B. Duke, *The Birth and Evolution of Surface Science: Child of the Union of Science and Technology*, PNAS **100**, 3858 (2003)

[2] H. Winick, S. Doniach (Eds.), *Synchrotron Radiation Research*, Plenum Press, New York (1980), Chapter 2

[3] B. Kasemo, *Biological surface science*, Surf. Sci. **500**, 656 (2002)

[4] D. F. Williams, *Corrosion of Implant Materials*, Annu. Rev. Mater. Sci. **6**, 237 (1976)

[5] A. P. Ameen, R. D. Short, R. Johns, G. Schwach, *The Surface Analysis of Implant Materials*, Clin. Oral. Impl. Res. **4**, 144 (1993)

[6] A. Arys, C. Philippart, N. Dourov, Y. He, Q. T. Le, J. J. Pireaux, *Analysis of Titanium Dental Implants after Failure of Osseointegration: Combined Histological, Electron Microscopy, and X-ray Photoelectron Spectroscopy Approach*, J. Biomed. Mater. Res. B **43**, 300 (1998)

[7] T. Albrektsson, P.-I. Brånemark, H.-A. Hansson, B. Kasemo, K. Larsson, I. Lundström, D. H. McQueen, R. Skalak, *The interface zone of inorganic implants in vivo: titanium implants in bone*, Ann. Biomed. Eng. **11**, 1 (1983)

[8] B. E. Nieuwenhuys, *The surface science approach toward understanding automotive exhaust conversion catalysis at the atomic level*, Adv. Catal. **44**, 295 (1999)

[9] M. Bowker, *The basis and applications of heterogeneous catalysis*, Oxford University Press Inc., New York (1998), Chapter 8

[10] M. Haruta, N. Yamada, T. Kobayashi, S. Iijima, *Gold catalysts prepared by coprecipitation for low-temperature oxidation of hydrogen and of carbon monoxide*, J. Catal. **115**, 301 (1989)

[11] A. Cho, *Connecting the dots to custom catalysts*, Science **299**, 1684 (2003)

[12] C. E. J. Mitchell, A. Howard, M. Carney, R. G. Egdell, *Direct observation of behavior of Au nanoclusters on TiO_2(110) at elevated temperatures*, Surf. Sci. **490**, 196 (2001)

[13] M. Valden, X. Lai, D. W. Goodman, *Onset of catalytic activity of gold clusters on titania with the appearance of nonmetallic properties*, Science **281**, 1647 (1998)

[14] N. S. Lewis, *Toward Cost-effective Solar Energy Use*, Science **315**, 798 (2007)

[15] M. Grätzel, *Dye-sensitized solar cells*, J. Photochem. Photobiol. C **4**, 145 (2003)

[16] B. O'Regan, M. Grätzel, *A low-cost, high efficiency solar cell based on dye-sensitized colloidal TiO_2 films*, Nature **353**, 737 (1991)

[17] J.-H. Yum, P. Chen, M. Grätzel, M. K. Nazeeruddin, *Recent Developments in Solid-State Dye-Sensitized Solar Cells*, ChemSusChem **1**, 699 (2008)

[18] http://nobelprize.org/nobel_prizes/physics/laureates/1921/

[19] http://nobelprize.org/nobel_prizes/physics/laureates/1981/

[20] J. J. Sakurai, *Modern Quantum Mechanics*, Addison-Wesley Publishing, Reading, Massachusetts (1994), Chapter 2

[21] C. Cohen-Tannoudji, B. Diu, F. Laloë, *Quantum Mechanics*, Hermann and John Wiley & Sons, Paris (1977), Complements of Chapter 7 AXIII

[22] S. Hüfner, *Photoelectron spectroscopy: principles and applications*, 3rd Edition, Springer, Berlin, Heidelberg (2003), Chapter 1

[23] N. Mårtensson, *Core Level Spectroscopies Applied to Surfaces and Adsorbates*, Ecole polytechnique fédérale de Lausanne, Lausanne (1994)

[24] W. F. Egelhoff, *Core-Level Binding-Energy Shifts at Surfaces and in Solids*, Surf. Sci. Rep. **6**, 253 (1987) and references therein.

[25] W. Schattke, M. A. Van Hove (Eds.), *Solid-state Photoemission and Related Methods: Theory and Experiment*, Wiley-VCH, Weinheim (2003)

[26] http://nobelprize.org/nobel_prizes/physics/laureates/1981/siegbahn-lecture.pdf

[27] A. Jablonski, C. J. Powell, *Relationships between electron inelastic mean free paths, effective attenuation lengths, and mean escape depths*, J. Electron. Spectrosc. Relat. Phenom. **100**, 137 (1999)

[28] J. F. Watts, J. Wolstenholme, *An Introduction to Surface Analysis by XPS and AES*, John Wiley & Sons, Chichester, West Sussex (2003), Chapter 3

[29] D. A. Shirley, *High-Resolution X-ray Photoemission Spectrum of the Valence Bands of Gold*, Phys. Rev. B **5**, 4709 (1972)

[30] M. Coville, T. D. Thomas, *Molecular effects on inner-shell lifetimes: Possible test of the one-center model of Auger decay*, Phys. Rev. A **43**, 6053 (1991)

[31] J. L. Campbell, T. Papp, *Widths of the Atomic K–N7 Levels*, At. Data Nucl. Data Tables **77**, 1 (2001)

[32] S. Doniach, M. Šunjić, *Many-electron singularity in X-ray photoemission and X-ray line spectra from metals*, J Phys. C **3**, 285 (1970)

[33] F. W. Lytle, *The EXAFS family tree: a personal history of the development of extended X-ray absorption fine structure*, J. Synchrotron Radiat. **6**, 123 (1999)

[34] J. Stöhr, *NEXAFS Spectroscopy*, Springer, Berlin, Heidelberg (1992), Chapter 3

[35] M. O. Krause, *Atomic Radiative and Radiationless Yields for K and L Shells*, J. Phys. Chem. Ref. Data **8**, 307 (1979)

[36] G. Hähner, *Near edge X-ray absorption fine structure spectroscopy as a tool to probe electronic and structural properties of thin organic films and liquids*, Chem. Soc. Rev. **35**, 1244 (2006)

[37] http://nobelprize.org/nobel_prizes/physics/laureates/1986/rohrer-lecture.pdf

[38] G. Binnig, H. Rohrer, *Scanning tunneling microscopy*, Helv. Phys. Acta **55**, 726 (1982)

[39] G. Binning, H. Rohrer, C. Gerber, E. Weibel, *Surface Studies by Scanning Tunneling Microscopy*, Phys. Rev. Lett. **49**, 57 (1982)

[40] G. Binning, H. Rohrer, C. Gerber, E. Weibel, *7x7 Reconstruction on Si(111) Resolved in Real Space*, Phys. Rev. Lett. **50**, 120 (1983)

[41] http://nobelprize.org/nobel_prizes/physics/laureates/1986/

[42] C. B. Duke, *Tunneling in Solids*, Academic Press, New York (1969), Chapter II

[43] J. Bardeen, *Tunneling from a many-particle point of view*, Phys. Rev. Lett. **6**, 57 (1961)

[44] C. J. Chen, *Introduction to Scanning Tunneling Microscopy*, Oxford University Press, New York (1993), Chapter 2

[45] A. D. Gottlieb, L. Wesoloski, *Bardeen's tunneling theory as applied to scanning tunneling microscopy: a technical guide to the traditional interpretation*, Nanotechnology **17**, R57 (2006)

[46] J. Tersoff, D. R. Hamann, *Theory and application for the scanning tunneling microscope*, Phys. Rev. Lett. **50**, 1998 (1983)

[47] J. Tersoff, D. R. Hamann, *Theory of the scanning tunneling microscope*, Phys. Rev. B **31**, 85 (1985)

[48] W. A. Hofer, *Challenges and errors: interpreting high resolution images in scanning tunneling microscopy*, Prog. Surf. Sci. **71**, 147 (2003)

[49] G. A. D. Briggs, A. J. Fisher, *STM experiment and atomistic modeling hand in hand: individual molecules on semiconductor surfaces*, Surf. Sci. Rep. **33**, 1 (1999)

[50] Omicron Vakuumphysik GmbH, Taunusstein, Germany

[51] M. Head-Gordon, E. Artacho, *Chemistry on the computer*, Phys. Today **61**, 58 (2008)

[52] P. Hohenberg, W. Kohn, *Inhomogeneous Electron Gas*, Phys. Rev. **136**, B864 (1964)

[53] W. Kohn, L. J. Sham, *Self-Consistent Equations Including Exchange and Correlation Effects*, Phys. Rev. **140**, A1133 (1965)

[54] http://nobelprize.org/nobel_prizes/chemistry/laureates/1998/

[55] W. Koch, M. C. Holthausen, *A Chemist's Guide to Density Functional Theory*, 2nd Edition, Wiley-VCH, Weinheim (2001), Chapter 1

[56] From Equations (2.16) to (2.20), Chapters 4 and 5 of reference [55] is followed.

[57] Axel Groβ, *Theoretical Surface Science A Microscopic Perspective*, Springer, Berlin, Heidelberg (2009), Chapter 3

[58] A. Michaelides, M. Scheffler, *An Introduction to the Theory of Crystalline Elemental Solids and their Surfaces*, in: *Textbook of Surface and Interface Science, Volume I*, Ed. K. Wandelt, (in press)

[59] M. C. Payne, M. P. Teter, D. C. Allan, T. A. Arias, J. D. Joannopoulos, *Iterative minimization techniques for ab initio total-energy calculations: molecular dynamics and conjugate gradients*, Rev. Mod. Phys. **64**, 1045 (1992)

[60] M. D. Segall, P. J. D. Lindan, M. J. Probert, C. J. Pickard, P. J. Hasnip, S. J. Clark, M. C. Payne, *First-principles simulation: ideas, illustrations and the CASTEP code*, J. Phys. Condens. Matter **14**, 2717 (2002)

[61] D. Vanderbilt, *Soft self-consistent pseudopotentials in a generalized eigenvalue formalism*, Phys. Rev. B **41**, 7892 (1990)

[62] www.castep.org

[63] U. Diebold, *The surface science of titanium dioxide*, Surf. Sci. Rep. **48**, 53 (2003)

[64] M. Ramamoorthy, D. Vanderbilt, R. D. King-Smith, *First-principles calculations of the energetics of stoichiometric TiO_2 surfaces*, Phys. Rev. B **49**, 16721 (1994)

[65] W. Göpel, J. A. Anderson, D. Frankel, M. Jaehnig, K. Phillips, J. A. Schäfer, G. Rocker, *Surface defects of TiO_2(110): A combined XPS, XAES AND ELS study*, Surf. Sci. **139**, 333 (1984)

[66] N. G. Petrik, Z. Zhang, Y. Du, Z. Dohnlek, I. Lyubinetsky, G. A. Kimmel, *Chemical Reactivity of Reduced TiO_2(110): The Dominant Role of Surface Defects in Oxygen Chemisorption*, J. Phys. Chem. C **113**, 12407 (2009)

[67] C. M. Yim, C. L. Pang, G. Thornton, *Oxygen Vacancy Origin of the Surface Band-Gap State of TiO_2(110)*, Phys. Rev. Lett. **104**, 036806 (2010)

[68] C. M. Yim, C. L. Pang, G. Thornton, *A Reply to the Comment by S. Wendt et al.*, Phys. Rev. Lett. **104**, 259704 (2010)

[69] S. Wendt, P. T. Sprunger, E. Lira, G. K. H. Madsen, Z. Li, J. Ø. Hansen, J. Matthiesen, A. Blekinge-Rasmussen, E. Lægsgaard, B. Hammer, F. Besenbacher, *The Role of Interstitial Sites in the Ti3d Defect State in the Band Gap of Titania*, Science **320**, 1755 (2008)

[70] Z. Zhang, J. Lee, J. T. Yates Jr., R. Bechstein, E. Lira, J. Ø. Hansen, S. Wendt, F. Besenbacher, *Unraveling the Diffusion of Bulk Ti Interstitials in Rutile TiO_2(110) by Monitoring Their Reaction with O Adatoms*, J. Phys. Chem. C **114**, 3059 (2010)

[71] S. Wendt, R. Bechstein, S. Porsgaard, E. Lira, J. Ø. Hansen, P. Huo, Z. Li, B. Hammer, F. Besenbacher, *Comment on "Oxygen Vacancy Origin of the Surface Band-Gap State of TiO_2(110)"*, Phys. Rev. Lett. **104**, 259703 (2010)

[72] A. Kiejna, T. Pabisiak, S. W. Gao, *The energetics and the structure of rutile TiO_2(110)*, J. Phys. Condens. Matter **18**, 4207 (2006)

[73] P. J. D. Lindan, N. M. Harrison, M. J. Gillan, J. A. White, *First-principles spin-polarized calculations on the reduced and reconstructed TiO_2(110) surface*, Phys. Rev. B **55**, 15919 (1997)

[74] C. Di Valentin, G. Pacchioni, A. Selloni, *Electronic Structure of Defect States in Hydroxylated and Reduced Rutile TiO_2(110) Surfaces*, Phys. Rev. Lett. **97**, 166803 (2006)

[75] U. Diebold, J. Lehman, T. Mahmoud, M. Kuhn, G. Leonardelli, W. Hebenstreit, M. Schmid, P. Varga, *Intrinsic defects on a TiO_2(110) (1×1) surface and their reaction with oxygen: a scanning tunneling microscopy study*, Surf. Sci. **411**, 137 (1998)

[76] T. Minato, Y. Sainoo, Y. Kim, H. S. Kato, K.-I. Aika, M. Kawai, J. Zhao, H. Petek, T. Huang, W. He, B. Wang, Z. Wang, Y. Zha, J. Yang, J. G. Hou, *The electronic structure of oxygen atom vacancy and hydroxyl impurity defects on titanium dioxide (110) surface*, J. Chem. Phys. **130**, 124502 (2009)

[77] J. Ahdjoudj, C. Minot, *A theoretical study of HCO_2H adsorption on TiO_2(110)*, Catal. Lett. **46**, 83 (1997)

[78] S. P. Bates, G. Kresse, M. J. Gillan, *The adsorption and dissociation of ROH molecules on TiO_2(110)*, Surf. Sci. **409**, 336 (1998)

[79] P. Käckell, K. Terakura, *Dissociative adsorption of formic acid and diffusion of formate on the TiO_2(110) surface the role of hydrogen*, Surf. Sci. **461**, 191 (2000)

[80] L.-Q. Wang, K. F. Ferris, A. N. Shultz, D. R. Baer, M. H. Engelhard, *Interactions of HCOOH with stoichiometric and defective TiO_2(110) surfaces*, Surf. Sci. **380**, 352 (1997)

[81] A. S. Foster, R. M. Nieminen, *Adsorption of acetic and trifluoroacetic acid on the TiO_2(110) surface*, J. Chem. Phys. **121**, 9039 (2004)

[82] A. Fahmi, C. Minot, P. Fourre, P. Nortier, *A theoretical study of the adsorption of oxalic acid on TiO_2*, Surf. Sci. **343**, 261 (1995)

[83] L. Patthey, H. Rensmo, P. Persson, K. Westermark, L. Vayssieres, A. Stashans, Å. Petersson, P. A. Brühwiler, H. Siegbahn, S. Lunell, N. Mårtensson, *Adsorption of bi-isonicotinic acid on rutile TiO_2(110)*, J. Chem. Phys. **110**, 5913 (1999)

[84] J. Schnadt, J. Schiessling, J. N. O'Shea, S. M. Gray, L. Patthey, M. K.-J. Johansson, M. Shi, J. Krempaský, J. Åhlund, P. G. Karlsson, P. Persson, N. Mårtensson, P. A. Brühwiler, *Structural study of adsorption of isonicotinic acid and related molecules on rutile TiO_2(110) I: XAS and STM*, Surf. Sci. **540**, 39 (2003)

[85] J. Schnadt, J.N. O'Shea, L. Patthey, J. Schiessling, J. Krempaský, M. Shi, N. Mårtensson, P.A. Brühwiler, *Structural study of adsorption of isonicotinic acid and related molecules on rutile TiO_2(110) II: XPS*, Surf. Sci. **544**, 74 (2003)

[86] L. Ojamäe, C. Aulin, H. Pedersen, P.-O. Käll, *IR and quantum-chemical studies of carboxylic acid and glycine adsorption on rutile TiO_2 nanoparticles*, J. Colloid Interface Sci. **296**, 71 (2006)

[87] T. J. Lerotholi, E. A. Kröger, M. J. Knight, W. Unterberger, K. Hogan, D. C. Jackson, C. L. A. Lamont, D. P. Woodruff, *Adsorption structure of glycine on TiO_2(110): A photoelectron diffraction determination*, Surf. Sci. **603**, 2305, (2009)

[88] T. Qiu, M. A. Barteau, *STM study of glycine on TiO_2(110) single crystal surfaces*, J. Colloid Interface Sci. **303**, 229 (2006)

[89] A. G. Thomas, W. R. Flavell, C. P. Chatwin, A. R. Kumarasinghe, S. M. Rayner, P. F. Kirkham, D. Tsoutsou, T. K. Johal, S. Patel, *Adsorption of phenylalanine on single crystal rutile TiO_2(110) surface*, Surf. Sci. **601**, 3828 (2007)

[90] G. J. Fleming, K. Adib, J. A. Rodriguez, M. A. Barteau, J. M. White, H. Idriss, *The adsorption and reactions of the amino acid proline on rutile TiO_2(110) surfaces*, Surf. Sci. **602**, 2029 (2008)

[91] G. H. Vurens, M. Salmeron, G. A. Somorjai, *Structure, composition and chemisorption studies of thin ordered iron oxide films on platinum (111)*, Surf. Sci. **201**, 129 (1988)

[92] H.C. Galloway, J.J. Benítez, M. Salmeron, *The structure of monolayer films of FeO on Pt(111)*, Surf. Sci. **298**, 127 (1993)

[93] W. Ranke, M. Ritter, W. Weiss, *Crystal structures and growth mechanism for ultrathin films of ionic compound materials: FeO(111) on Pt(111)*, Phys. Rev. B **60**, 1527 (1999)

[94] G. Rupprechter, *Catalysis by Noble Metal Nanoparticles Supported on Thin-Oxide Films*, in: *Model Systems in Catalysis Single Crystals to Supported Enzyme Mimics*, Ed. Robert M. Rioux, Springer, Berlin, Heidelberg (2010)

[95] Y. J. Kim, C. Westphal, R. X. Ynzunza, H. C. Galloway, M. Salmeron, M. A. Van Hove, C. S. Fadley, *Interlayer interactions in epitaxial oxide growth: FeO on Pt(111)*, Phys. Rev. B **55**, R13448 (1997)

[96] L. R. Merte, J. Knudsen, L. C. Grabow, R. T. Vang, E. Lægsgaard, M. Mavrikakis, F. Besenbacher, *Correlating STM contrast and atomic-scale structure by chemical modification: Vacancy dislocation loops on FeO/Pt(111)*, Surf. Sci. **603**, L15 (2009)

[97] L. R. Merte, L. C. Grabow, G. Peng, J. Knudsen, H. Zeuthen, W. Kudernatsch, S. Porsgaard, E. Lægsgaard, M. Mavrikakis, F. Besenbacher, *Tip-Dependent Scanning Tunneling Microscopy Imaging of Ultrathin FeO Films on Pt(111)*, J. Phys. Chem. C **115**, 2089 (2011)

[98] M. Schmidt, S. G. Steinemann, *XPS studies of Amino Acids Adsorbed on Titanium Dioxide Surface*, Fresenius J. Anal. Chem. **341**, 412 (1991)

[99] K. Uvdal, P. Bodö, B. Liedberg, *L-Cysteine Adsorbed on Gold and Copper: An X-Ray Photoelectron Spectroscopy Study*, J. Colloid Interface Sci.**149**, 162 (1992)

[100] G. Dodero, L. De Michieli, O. Cavalleri, R. Rolandi, L. Oliveri, A. Dacca, R. Parodi, *L-Cysteine chemisorption on gold: an XPS and STM study*, Colloids and Surfaces A **175**, 121 (2000)

[101] O. Cavalleri, L. Oliveri, A. Dacca, R. Parodi, R. Rolandi, *XPS measurements on L-cysteine and 1-octadecanethiol self-assembled films: a comparative study*, Appl. Surf. Sci. **175-176**, 357 (2001)

[102] O. Cavalleri, G. Gonella, S. Terreni, M. Vignolo, P. Pelori, L. Floreano, A. Morgante, M. Canepa, R. Rolandi, *High resolution XPS of the S 2p core level region of the L-cysteine/gold interface*, J. Phys. Condens. Matter **16**, S2477 (2004)

[103] G. Gonella, S. Terreni, D. Cvetko, A. Cossaro, L. Mattera, O. Cavalleri, R. Rolandi, A. Morgante, L. Floreano, M. Canepa, *Ultrahigh Vacuum Deposition of L-Cysteine on Au(110) Studied by High-Resolution X-ray Photoemission: From Early Stages of Adsorption to Molecular Organization*, J. Phys. Chem. B **109**, 18003 (2005)

[104] E. Mateo Marti, C. Methivier, C. M. Pradier, *(S)-Cysteine chemisorption on Cu(110), from the gas or liquid phase: an FT-RAIRS and XPS study*, Langmuir **20**, 10223 (2004)

[105] J. W. Kim, H.-N. Hwang, C.-C. Hwang, *Adsorption of Cysteine on Cu(110) Studied by Core-Level Photoelectron Spectroscopy*, J. Phys. Chem. C **111**, 13192 (2007)

[106] Thomsen, M. T. Wharmby, D. P. Riley, G. Held, M. J. Gladys, *The adsorption and stability of sulfur containing amino acids on Cu{531}*, Surf. Sci. **603**, 1253 (2009)

[107] A. P. J. Stampfl, C.-H. Chen, S.-C. Wang, M.-L. Huang, R. Klauser, *A scanning photoemission microprobe study of the adsorption of cysteine on Pt{111}*, J. Electron. Spectrosc. Relat. Phenom. **144–147**, 417 (2005)

[108] D. S. Martin, G. E. Isted, R. J. Cole, P. Weightman, *Investigating the adsorption of the amino acid L-cysteine onto Ag(110)*, Phys. Status Solidi C **2**, 4043 (2005)

[109] J. W. Kim, Y. M. Lee, S. M. Lee, M. J. Son, H. Kang, Y. Park, *Surface Reaction of Sulfur-Containing Amino Acids on Cu(110)*, Langmuir **26**, 5632 (2010)

[110] B. Meunier, *Metalloporphyrins as versatile catalysts for oxidation reactions and oxidative DNA cleavage*, Chem. Rev. **92**, 1411 (1992)

[111] R. Purrello, S. Gurrieri, R. Lauceria, *Porphyrin assemblies as chemical sensors*, Coord. Chem. Rev. **190-192**, 683 (1999)

[112] J. A. A. W. Elemans, R. van Hameren, R. J. M. Nolte, A. E. Rowan, *Molecular Materials by Self-Assembly of Porphyrins, Phthalocyanines, and Perylenes*, Adv. Mater. **18**, 1251 (2006)

[113] L. Fu, L. Cao, Y. Liu, D. Zhu, *Molecular and nanoscale materials and devices in electronics*, Adv. Colloid Interface Sci. **111**, 133 (2004)

[114] B. Hammer, J. K. Norskov, *Why gold is the noblest of all the metals*, Nature **376**, 238 (1995)

[115] M. Haruta, *Size- and support-dependency in the catalysis of gold*, Catal. Today **36**, 153 (1997)

[116] M. Haruta, S. Tsubota, T. Kobayashi, H. Kageyama, M. J. Genet, B. Delmon, *Low-Temperature Oxidation of CO over Gold Supported on TiO_2, α-Fe_2O_3, and Co_3O_4*, J. Catal. **144**, 175 (1993)

[117] F. Yang, M. S. Chen, D. W. Goodman, *Sintering of Au Particles Supported on TiO_2 (110) during CO Oxidation*, J. Phys. Chem. C **113**, 254 (2009)

[118] A. Cao, R. Lu, G. Veser, *Stabilizing metal nanoparticles for heterogeneous catalysis*, PCCP **12**, 13499 (2010)

[119] O. Lopez-Acevedo, K. A. Kacprzak, J. Akola, H. Häkkinen, *Quantum size effects in ambient CO oxidation catalysed by ligand-protected gold clusters*, Nat. Chem. **2**, 329 (2010)

[120] M.-C. Daniel, D. Astruc, *Gold Nanoparticles: Assembly, Supramolecular Chemistry, Quantum-Size-Related Properties, and Applications toward Biology, Catalysis, and Nanotechnology*, Chem. Rev. **104**, 293 (2004)

[121] M. Boronat, F. Illas, A. Corma, *Active Sites for H_2 Adsorption and Activation in Au/TiO_2 and the Role of the Support*, J. Phys. Chem. A **113**, 3750 (2009)

[122] T. Pabisiak, A. Kiejna, *First-principles study of Au nanostructures on rutile TiO_2(110)*, Phys. Rev. B **79**, 085411 (2009)

[123] S. Laursen, S. Linic, *Strong Chemical Interactions Between Au and Off-Stoichiometric Defects on TiO_2 as a Possible Source of Chemical Activity of Nanosized Au Supported on the Oxide*, J. Phys. Chem. C **113**, 6689 (2009)

[124] D. Matthey, J. G. Wang, S. Wendt, J. Matthiesen, R. Schaub, E. Laegsgaard, B. Hammer, F. Besenbacher, *Enhanced Bonding of Gold Nanoparticles on Oxidized TiO_2(110)*, Science **315**, 1692 (2007)

[125] L. Zhang, R. Persaud, T. Madey, *Ultrathin metal films on a metal oxide surface: Growth of Au on TiO_2(110)*, Phys. Rev. B **56**, 10549 (1997)

[126] A. Howard, D. N. S. Clark, C. E. J. Mitchell, R. G. Egdell, V. R. Dhanak, *Initial and final state effects in photoemission from Au nanoclusters on TiO_2(110)*, Surf. Sci. **518**, 210 (2002)

[127] T. Minato, T. Susaki, S. Shiraki, H. S. Kato, M. Kawai, K.-I. Aika, *Investigation of the electronic interaction between TiO_2(110) surfaces and Au clusters by PES and STM*, Surf. Sci. **566–568**, 1012 (2004)

[128] T. Okazawa, M. Fujiwara, T. Nishimura, T. Akita, M. Kohyama, Y. Kido, *Growth mode and electronic structure of Au nano-clusters on NiO(001) and TiO_2(110)*, Surf. Sci. **600**, 1331 (2006)

[129] T. Okazawa, M. Kohyama, Y. Kido, *Electronic properties of Au nano-particles supported on stoichiometric and reduced TiO_2(110) substrates*, Surf. Sci. **600**, 4430 (2006)

[130] Z. Jiang, W. Zhang, L. Jin, X. Yang, F. Xu, J. Zhu, W. Huang, *Direct XPS Evidence for Charge Transfer from a Reduced Rutile TiO_2(110) Surface to Au Clusters*, J. Phys. Chem. C **111**, 12434 (2007)

[131] J.G. Tao, J. S. Pan, C. H. A. Huan, Z. Zhang, J. W. Chai, S. J. Wang, *Origin of XPS binding energy shifts in Ni clusters and atoms on rutile TiO_2 surfaces*, Surf. Sci. **602**, 2769 (2008)

[132] J. S. Pan, J. G. Tao, C. H. A. Huan, S. Y. Chiam, Z. Zhang, D. T. H. Li, Y. Sun, J. W. Chai, S. J. Wang, C. Q. Sun, *Determination of atomic Ni interaction with TiO_2 by XPS*, Surf. Interface Anal. **42**, 878 (2010)

[133] P. S. Bagus, A. Wieckowski, H. Freund, *Initial and final state contributions to binding-energy shifts due to lattice strain: Validation of Auger parameter analyses*, Chem. Phys. Lett. **42**, 420 (2006)

Chapter 7

Acknowledgments

Trying to categorize everything is one of my addictions. To acknowledge people I will use the same approach. This approach results some inconsistencies since some people's names show up more than once, however, this is the only chapter of the thesis where inconsistencies occur.

The first group consists of people without whom this thesis could not exist. My supervisors, **Jesper N. Andersen** and **Joachim Schnadt**, by first giving me the opportunity of a PhD education and second teaching and supporting me with their knowledge and experience during my education, take the first place. My colleagues, **Cristina Isvoranu**, **Jan Knudsen** *and* **Javier Carrasco**, and **Karina Schulte**, by helping me to carry out the actual research activities and supporting me both mentally and scientifically, take the second place. The financial sources, European Commission through the **MONET** Early Stage Researcher Training Network and **Lund University**, take the third place.

The second group consists of people without whom this thesis would still exist but could be less shiny: our distant collaborators, **Anna Rienzo**, **Graziano Magnano**, and **James O'Shea**, take the first place. **Joachim Schnadt** and **Jan Knudsen**, by reading the manuscripts very carefully, correcting my poor grammar and complicated sentences and coming up with scientifically valuable suggestions, share the first place.

The third group consists of people without whom I could not have learnt how to do DFT calculations. My supervisors, **Jesper N. Andersen** and **Joachim Schnadt**, for trusting me and giving me the opportunity to do DFT, and **Angelos Michaelides**, for teaching me almost 70% of the things that I know about DFT within two days, take the first place. **Javier Carrasco**, by answering all my stupid questions with patience and supporting me when any kind of technical problem occurred, takes the second place.

The fourth group consists of people without whom the working conditions could be very harsh. My colleagues **Cristina Isvoranu** and **Jan Knudsen** take the first place. All current and former members of Division of Synchrotron Radiation Research, especially my office mates, and nice MAX-lab people, take the second place.

The fifth group consists of people without whom life and therefore a PhD education would be meaningless. My father **Atilla**, mother **Zeliha**, and brother **İsmail Ataman**, take the first place. I also would like to thank to min älskling **Catharina Lindell** for supporting me since almost one year in many different ways but mostly saying "everything is going to be okay, don't worry".

And finally the one who can not be categorized, thanks to God.